MATCH
Communications in Mathematical and in Computer Chemistry

MATCH Commun. Math. Comput. Chem. **84** (2020) 85-130

ISSN 0340 - 6253

Advanced Distributed Reactivity Model for the Static Pyrolysis of Corn Stover Feedstock

Nebojša Manić[1,*], Bojan Janković[2], Hadi Waisi[2], Dragoslava Stojiljković[1], Miloš Radojević[1]

[1]*University of Belgrade, Faculty of Mechanical Engineering, Fuel and Combustion Laboratory, Kraljice Marije 16, P.O. Box 35, 11120 Belgrade, Serbia*

[2]*University of Belgrade, Institute of Nuclear Sciences "Vinča", Department of Physical Chemistry, Mike Petrovića Alasa 12-14, P.O. Box 522, 11001 Belgrade, Serbia*

(Received June 3, 2019)

Abstract

Advanced distributed reactivity model for static pyrolysis of corn stover was proposed. It was found that at the lowest operating temperature (180 °C), pyrolysis process was governed by autocatalytic and non-autocatalytic reactions which occur simultaneously. With an increasing of the operating temperature above 180 °C, the amplifying of acceleratory behavior of the process was observed, where at 270 °C a fairly rapid surface reactions dominate. It was established that surface reaction geometry activities become dominant at highest operating temperature. It was found that retention of the apparent activation energy (E_a) at low level probably originates from mineral content linked to ash, which has harmful effect on volatiles yield. Based on estimated characteristic features of reactivity distribution, it was concluded that with an increasing of operating temperature we have a reduction in a char yield, and an increase in gas yield. Proposed model enables identification of chemical compounds that first undergoes in decomposition during pyrolysis.

[*] *Corresponding Author*.

E-mail address: nmanic@mas.bg.ac.rs (N. Manić).

Nomenclature

TGA - thermogravimteric analysis

TG – thermogravimetry

TA – thermo-analytical

CS - corn stover

RRCM - the reaction rate constant method

DAEM – distribution of activation energy model or distributed activation energy model

MC - moisture content (%)

ASTM - The American Society for Testing and Materials

HHV – the higher heating value (MJ kg^{-1})

ddf – the density distribution function

SB - Šesták-Berggren model

SSRE - the sum of square of relative error (%)

φ – the gas flow rate (mL min^{-1})

T_i – the *i*-th operating temperature (°C)

α – reacted fraction of the sample (conversion)

(1-α) - the un-reacted fraction

α_p - the conversion value which corresponds to the peak of the rate process curve

A - the pre-exponential factor (min^{-1})

E_a - the apparent activation energy (J mol^{-1})

T – the absolute temperature (K)

R - the gas constant (J K^{-1} mol^{-1})

f(α) - the function of the reaction model

Ω – the objective function

Dev - deviation between observed and calculated conversion curves (%)

N - the number of data points

ρ - the number of parameters employed in the model

c_i – the contribution of pseudo-component *i* to the total mass loss

i - the component index

g(α) - the integral form of the reaction model

α(*t*) - the time-dependent extent of conversion

t - the time (min)

k - the overall rate constant (min^{-1})

m - the Avrami's exponent

k_o - the constant (min^{-1})

n_{Local} – the local Avrami's exponent

$t_{0.50}$ - the reaction's half-life (min)

δ_i - the impingement factor

P(*t*) - the probability that the corresponding domain is empty of nucleation centers

η^* - the correlation parameter

$f(E_a)_{exp}$ – the experimental density distribution function (mol $(kJ)^{-1}$)

Δm_{res} - the residual mass loss (%)

$\langle E_a \rangle$ - average value of the apparent activation energy (kJ mol^{-1})

Ψ - the fractal dimension constant

$F(E_a)$ – the cumulative probability function

μ - the mean (expected) value (kJ mol^{-1})

σ - standard deviation (dispersion) (kJ mol^{-1})

N^* - the number of reactions in a series

t_N - the random times of decompositions from the Weibull distribution (min)

$\ln(t_N)$ - the random times of decompositions from the Extreme distribution (t_N in min)

$f_W(E_a)$ – the Weibull density distribution function (mol $(kJ)^{-1}$)

β – the Weibull shape parameter

η – the Weibull scale parameter (kJ mol^{-1})

$F_W(E_a)$ – the Weibull cumulative distribution function

1 Introduction

Thermochemical conversion of biomass to gaseous and liquid fuels is an alternative route to meet the energy demands on a sustainable basis. The gasification and pyrolysis are the two main thermochemical conversion techniques for the biomass. The pyrolysis produces mostly liquid fuel, the pyrolytic oil or bio-oil, in the absence of oxidizing agent, while gasification produces mainly gaseous fuel in the presence of an oxidizing agent [1,2]. The pyrolysis of lignocellulosic materials is a promising route for converting the renewable feedstocks to the transportation fuel. These materials include agricultural wastes, such as the corn stover. Agricultural wastes are renewable and carbon dioxide neutral feedstock. Besides landfill disposal, many different processes have been considered for utilizing biomass wastes: combustion (incineration), aerobic and anaerobic biodigestion, wet oxidation, supercritical oxidation, steam reforming, etc. [3]. While many pyrolysis studies have been done on the biomass materials, most of these have focused on the production of liquid fuels, chemicals, or the hydrogen [4,5], and not the fuel gas mixtures (H_2, CO, CH_4). On the laboratory scale-grade level, the thermoanalytical techniques are often used in the study of biomass pyrolysis. The use of thermogravimteric analysis (TGA) in the study of pyrolysis behavior of biomass has been reported in the literature [6-9].

Properties of a studied biomass material such as corn stover (usually consists of the leaves, stalks, and cobs of maize (corn)) greatly influence the design and the operation of thermochemical conversion systems. In addition, commercial thermogravimteric systems have a high precision, the sample temperature is not directly measured or controlled. Depending on the temperature, heating rate regime, residence time, the pyrolysis process can be classified as flash, fast or slow. Flash pyrolysis involves rapid heating at temperatures ranging from 400 to 900 ^{o}C. Fast pyrolysis, on the other hand, occurs at temperatures lower than 600 ^{o}C and at not extremely high heating rates. Slow pyrolysis involves lower heating rates up to 450 or to 700 ^{o}C [10].

One of the challenges facing the sustainable production of renewable energy sources such as biomass is to develop an understanding of the reaction kinetics [11], when biomass is thermo-chemically converted to bio-fuel. It is common to assume that the pyrolytic decomposition of biomass and other carbonaceous fuels proceeds according to an infinitely large set of the first-order reactions, allowing the calculation of an overall, or the apparent activation energy (E_a) assuming an overall first-order reaction (or a series of reactions that sum to an overall first-order reaction). Innumerable studies of the biomass pyrolysis literature

calculate this activation energy using previously assumption, also known as the reaction rate constant method (RRCM) [12]. A large number of papers related to biomass pyrolysis studies show a reaction order of approximately unity. This assumption is commonly applied to account for the simultaneous reactions occurring during the pyrolysis of heterogeneous biomasses and is considered as a reasonable approximation given the high degree of linearity of the Arrhenius plots [13]. The kinetic models of biomass pyrolysis can be classified as the single reaction model and the multi-reaction model [11,14]. The frequently used kinetics model for investigating the pyrolysis process of lignocellulosic materials represents the DAEM (distribution of activation energy model) approach, that encompasses multiple reactions with different apparent activation energies. This approach using the various distribution functions in order to cover as good as possible the wide area of apparent activation energy variations [15-18].

However, many of these models fails to capture the entire range of the decomposition. The consequence of the inability to cover the entire range (in terms of the reaction coordinates) of decomposition, the most common causes of deviation from the simple first-order kinetics, which leads to a significant disturbing of data in the Arrhenius plot. This phenomenon can cause bending of the Arrhenius plot as a concave downwards or the upwards. Consequently, this may lead to emerging of complex nature of pyrolytic process, where various decomposition regions which includes the devolatilization primarily hemicellulose, cellulose and lignin may overlap, where a first- order approximation is no longer valid. Therefore, it is necessary to implement a new model where these changes can be more easily identified, and where a more realistic kinetic model can provide us the detailed mechanistic scheme of this extremely complex heterogeneous process for the biomass system which is turned on with a complicated composition. Some of the important guidelines for accurate determination of kinetic parameters for the complex heterogeneous processes have been previously reported in the literature [19].

The main objective of this study was to obtain a more flexible kinetic model for pyrolysis of dried corn stover under static experimental conditions using thermo-analytical (TA) technique. A new kinetics model which describes pyrolytic behavior of corn stover (in a narrow temperature range ΔT = 180 – 270 ^{o}C) monitored by thermogravimetry (TG) was proposed. The model is based on the combined kinetic and statistical approach, with physical connection between kinetic and statistical parameters that would provide a clearer mechanistic picture of the process. The low-temperature range pyrolysis process under controlled ramping program (static experimental conditions) up to 300 ^{o}C is important from product yields point

of view. Namely, it can be noted that below 300 ^{o}C, the products of pyrolysis are generally expected largely to contain bio-char, bio-oil and syngas. However, the phase distribution and chemical composition of the products is highly dependent on the feedstock used as well as the operating parameters of the process. The operating conditions have a strong impact on the products formed. The operating temperature range applied in this work corresponds to the temperatures (maximum up to T = 500 ^{o}C) used in rotary klin pyrolysis reactors which have been successfully implemented on the industrial scale [20]. Because of these facts, the proposed kinetics approach was implemented in this work under the above-mentioned circumstances.

Also, one of the aims of this study is to compare biomass composition with physico-chemical characteristics (including statistically derived distribution of activation energy counterparts) of the system improved by model. Mathematical consideration of the proposed model can help to identify and assess environmentally sounded technologies for converting biomass into the valuable products. It can be pointed out that the essence of this paper is not the characterization analysis of pyrolysis products obtained at low temperatures, but rather a new mathematically developed model of low-temperature pyrolysis when it performed under temperature-ramping conditions. Almost all the current literature and applications of pyrolysis are focused on the high temperature and grounded feedstock. Pyrolysis at the high temperature is desirable due to the enhanced yield of gaseous compounds and bio-char, which contain high higher heating values. Those operating parameters, though, make most pyrolytic processes economically unviable, dangerous and they can also produce highly toxic gases which require treatment before they can be vented to the atmosphere. Taking into account all of these issues, one of the more noticeable effects of low temperature pyrolysis is the production of lower amounts of toxic gases, which is highly attractive. This provides an excellent opportunity for further development and research, so that the low temperature pyrolysis can be used at domestic scale with the least risks. To our knowledge, the kinetics operations to pyrolysis reactions which can occur at lower temperatures has not been yet considered and proposed approach was firstly implemented in this work for corn stover feedstock.

2 Materials and methods

2.1 Material

The corn stover samples used in the experiments were harvested from local farm in the autonomous province of "Vojvodina" in the Republic of Serbia. The biomass samples were harvested in the form of bales. The samples were initially ground to a bigger particle sizes using a 50.8 – mm screen with Vermeer HG200 horizontal grinder (Vermeer Corporation, Pella, USA). Grounded material was evaluated for moisture content and then stored in a sealed plastic container which were maintained at about T = 5 ºC until it was further size reduced to a 125 μm. The current conditions have been implemented due to dry to storable moisture concentration to prevent microbial decomposition. The moisture content (MC) is important factor with regard to effect of MC on the glass transition temperature of corn stover [21]. Particle size, along the moisture content, is one of the most significant factors affecting overall pellet quality.

2.2 Proximate and ultimate analyses

The data for proximate and ultimate analyses were obtained from LECO analytical (LECO Mac-400 TG analyzer, LECO CHN-2000 elemental determinator and LECO SC-132 sulfur determinator, respectively; LECO Corporation — a manufacturer of the analytical instrumentation, St. Joseph, Michigan, USA). For present studies, the LECO instrumentation contains easy to follow menu supported by Windows® based software, which allows these analysis methods. The analysis methods can also be entered to evaluate the moisture, volatiles, and ash content. The ASTM (The American Society for Testing and Materials) standard methods for estimating the chemical composition were used to measure the proximate and ultimate composition of studied biomass material [22-27]. For higher heating value (HHV) determination, the ASTM D5865 standard was used [28].

2.3 Static pyrolysis measurements

The static pyrolysis investigations of feedstock samples were carried out on a thermogravimetric (TG) analyzer (TA Instruments SDT 2960, TA Instruments, 159 Lukens Drive, New Castle, UK, DE 19720) device. For all feedstock samples, the value of the heating rate (in the use as fast as possible sample heating) used to achieve the desired operating temperature was 50 ºC min^{-1}. All thermogravimetric (TG) experiments were carried out in an atmosphere of the flowing nitrogen (the gas flow rate of φ = 50 mL min^{-1}). The feedstock

samples (towards the particle sizes of 125 μm after grinding with fine biomass feedstock splitter of IKA Laboratory process equipment (IKA® — Werke GmbH & Co., Janke & Kunkel-Str. 10, 79219 Staufen, Germany)) with the initial mass of 7-8 mg were taken in an open alumina crucible, where the crucible weight was calibrated to zero. The static thermogravimetric measurements were carried out at three different operating temperatures (T_i = 180, 230 and 270 ^{o}C (i = 3)). All pyrolytic measurements were repeated at actual operating temperatures until the consistency of the experimental data that has been identified.

3 Theoretical backgrounds

The kinetic analysis of the biomass thermal decomposition is usually based on the rate equation as:

$$\frac{d\alpha}{dt} = A\exp\left(-\frac{E_a}{RT}\right)\cdot f(\alpha), \tag{1}$$

where α represents the reacted fraction of the sample or conversion (α = (m_o - m_t)/(m_o - m_∞), where m_o is the initial (at t = 0) mass of the sample, m_t is the actual mass of the sample at any other time than t = 0 ($t \neq 0$), and m_∞ is the final ("equilibrium") mass of the sample, at $t = \infty$), A and E_a are the kinetic (Arrhenius) parameters, the pre-exponential factor (min^{-1}) and the apparent activation energy (J mol^{-1}), respectively, and $f(\alpha)$ is the function of the reaction model; T is the absolute temperature (K), and R is the gas constant (J K^{-1} mol^{-1}). These three parameters [A, E_a and $f(\alpha)$] are needed to provide a mathematical description of the biomass decomposition process and can be used to reproduce the original kinetic data and predict the process kinetics outside the experimental temperature region.

There are two main approaches for mathematical determination of these three parameters, namely the "model-fitting" and "model-free" or the isoconversional approaches.

The "model-fitting" approach is based on the initial assumption of a function for $f(\alpha)$ from a selection of available and well-known models [29], and fitting of the chosen model to experimental data in order to obtain the Arrhenius parameters. The classic application of "model-fitting" approach is to manipulate the differential or integral form of the rate equation untial a straight line plot can be obtained. The reaction model which gives the straightest line is selected and E_a and A are then obtained from the values of slope and intercept. The limitation of this classical "model-fitting" approach is that the data are very often over manipulated leading to a masking of errors in TG data.

In more recent times, owing in part to positive developments in computer technology including advanced software computational programs, the "model-fitting" approach has tended towards the use *non-linear least-square* analysis.

An algorithm developed within Matlab® code was used to obtain the optimal parameters that minimize, under constraints, the objective function, Ω, as:

$$\Omega = \sum_{j=1}^{j=N} \left[\left(\frac{d\alpha}{dt} \right)_j^{\exp} - \left(\frac{d\alpha}{dt} \right)_j^{calc} \right]^2, \tag{2}$$

where $(d\alpha/dt)^{exp}_j$ and $(d\alpha/dt)^{calc}_j$ represent the observed and calculated rate curves, for every *j*-th detected data point, respectively.

The deviation between the observed and calculated curves, at the optimal set of parameters, was calculated as follows:

$$Dev(\%) = 100 \times \frac{\sqrt{\Omega \cdot (N - \rho)}}{\max \left(\frac{d\alpha}{dt} \right)^{\exp}}, \tag{3}$$

where N represents the number of data points and ρ is the number of parameters employed in the model.

The decomposition of biomass is too complex to be realistically described using the single component model such in the Eq. (1), so a multi-component model can be assumed in "model-fitting" analysis. Actual material studied is assumed to be composed of the pseudo-components, which refer to a group of the reactive species that exhibit similar reactivity e.g., cellulose, hemicellulose, lignin, and extractives. In considered case, the Eq. (1) becomes:

$$\left(\frac{d\alpha_i}{dt} \right) = \sum c_i A_i \exp\left(-\frac{E_{ai}}{RT} \right) \cdot f(\alpha_i), \tag{4}$$

where c_i is the contribution of pseudo-component i to the total mass loss, i is the component index, A_i and E_{ai} are the Arrhenius parameters related to a given i-th pseudo-component, and α_i is the conversion ($0 < \alpha_i < 1$). The parameters calculated are linked to a specific reaction model assumed. The level of complexity may frequently arise where different reaction models are able to satisfactorily fit the experimental data, but the values of A and E_a may significantly different [30].

The isoconversional method does not require the choosing of a reaction model and is thus "model-free". It allows the estimation of E_a as a function of α, without assuming any particular form of the reaction model, $f(\alpha)$.

The main principle behind this approach is that the reaction rate for a constant extent of conversion varies only with the temperature.

The *integral* static isoconversional method is based on the integral form of the Eq. (1) ($g(\alpha) = A_\alpha \cdot \exp(- E_{a,\alpha}/RT) \cdot t_\alpha$, where $g(\alpha)$ is the integral form of the reaction model), than the simple rearrangement of above-mentioned equation leads us to application of the isoconversional principle in a form:

$$-\ln t_{\alpha,i} = \ln\left[\frac{A_\alpha}{g(\alpha)}\right] - \frac{E_{a,\alpha}}{RT_i}, \tag{5}$$

where $t_{\alpha,i}$ is the time to reach a given conversion at the different operating temperatures, T_i. Thus, the value of the apparent activation energy at a given α ($E_{a,\alpha}$) obtained by the isoconversional method is determined by the slope of the plot of $-\ln t_{\alpha,i}$ against $1/T_i$. This approach represents the standard integral isoconversional method [31] used under the static conditions.

To asses the $E_{a,\alpha} = E_{a,\alpha}(\alpha)$ dependence from the static data, the Friedman's [32] *differential* isoconversional method can be used. The Friedman's approach was based on the Eq. (1) in the logarithmic form such as:

$$\ln\left(\frac{d\alpha}{dt}\right)_{\alpha,i} = \ln\left[A_\alpha \cdot f(\alpha)\right] - \frac{E_{a,\alpha}}{RT_i}. \tag{6}$$

For $\alpha = const.$, the plot of $\ln(d\alpha/dt)_{\alpha,i}$ against $1/T_i$ obtained from the several isotherms should be a straight line whose slope allows to asses the apparent activation energy value at a given α ($E_{a,\alpha}$). However, both considered isoconversional methods do not compute a pre-exponential factor (A) nor determine a reaction model ($g(\alpha)$ or $f(\alpha)$). The Friedman's method is useful for studying the multi-step nature of biomass devolatilization and the corresponding dependence of the apparent activation energy (E_a), on the conversion, α.

Once the apparent activation energy (E_a) has been determined, the special functions $Y(\alpha)$ and $Z(\alpha)$ can be defined in order to determine the reaction model function, $f(\alpha)$. These special functions can be obtained by the simplified transformation procedure of the experimental data [33]:

$$Y(\alpha) = \left(\frac{d\alpha}{dt}\right) \approx f(\alpha), \tag{7}$$

$$Z(\alpha) = \left(\frac{d\alpha}{dt}\right) t = f(\alpha)\, g(\alpha). \tag{8}$$

In static conditions, however, the term related to the rate constant, $k = A \cdot \exp(-E_a/RT)$, in Eq. (1), is the constant, and the rate ($d\alpha/dt$) is proportional to $f(\alpha)$ function, as shown in Eq. (7). Therefore, if the reaction rate is plotted as a function of α, its shape corresponds to $f(\alpha)$ function. It is convenient to normalize $Y(\alpha)$ plot within [0,1] interval. The shape of this plot (with the maximum designated by α_M) is characteristic for each kinetic model and it can be used as the diagnostic tool, for determination of the kinetic model. It was shown [33] that maximum of $Z(\alpha)$ function (designated by α_p^{∞}) has characteristic values for the basic reaction models. The function $Z(\alpha)$ is useful for classification of possible reaction model, $f(\alpha)$ or $g(\alpha)$. Also, in practice, often applies that the function $Z(\alpha)$ is also normalized within [0,1] interval.

By the combination of the shape of function $Y(\alpha)$ with parameters α_M, α_p (the conversion value which corresponds to the peak of the rate process curve) and α_p^{∞} at which the function $Y(\alpha)$, the rate curve $d\alpha/dt$ *vs.* t and $Z(\alpha)$ have a maximum, respectively, the most suitable kinetic model function can be determined.

In addition, rather than fitting the data to one of a number of possible rate equations, and attempting to discern the rate controlling process by judging the goodness of fit between the data and each rate equation, it is possible to employ a general rate equation in which the function $f(\alpha)$ (Eq. (1)) is expressed in general manner with a variable parameter that reflects the rate controlling mechanism.

This type of equation is usually referred to the "empirical rate equation". One of the most famous of these equations is the Avrami's (or Johnson-Mehl-Avrami) equation [34]. For a long time, the Avrami's equation or its linearized equivalent, the Hancock and Sharp formalism [35] have been preferred in the publications dealing with the evaluation of the kinetic data concerning the formation of a solid from a liquid or from another solid. The Avrami's equation and its equivalent equation as described above may be presented in the following forms:

$$\alpha(t) = 1 - \exp\left[-(k \cdot t)^m\right], \tag{9}$$

and

$$\ln\left\{-\ln\left[1-\alpha(t)\right]\right\} = m \cdot \ln(k) + m \cdot \ln t, \tag{10}$$

where $\alpha(t)$ is the time-dependent extent of conversion, t is the time, k is the overall rate constant, and m represents the Avrami exponent. The exponent m reflects the nucleation rate and/or the growth mechanism. The term on the left-hand side of Eq. (9), $\alpha(t)$, represents from the standpoints of nucleation and growth theory, the volume of transformed fraction, while k is the thermally-activated rate constant.

The double logarithmic plot of ln{-ln[1-α(*t*)]} against ln*t* should give a straight line, the slope of which represents the order of reaction or the Avramii exponent, *m*. If the *single* process mechanism operates through the monitored operating temperature range in a given extent of conversion range, the evaluated plots represent a set of *parallel lines* with a constant or the approximately equal value of the Avrami exponent, *m*. The corresponding values of *m* for a range of established kinetic models were first presented by the Hancock and Sharp [35].

The rate constant *k* is the temperature-sensitive factor as $k = k_o \cdot \exp(-E_a/RT)$, where E_a is the single apparent activation energy value, while the k_o is a constant. It should be mentioned that if the Avrami analysis is valid, the value of *m* should not change with either the extent of conversion (α), or the operating temperature of considered process. It has been found that the usual approach of applying the Avrami's equation and calculating the mean value of the Avrami exponent over the entire range of α's, may be inappropriate, even misleading, if competing reactions or changes in the growth dimensionality occur during the decomposition progress. Also, a close examination of the plots derived from Eq. (10) reveals that there are deviations from the linearity over the full range of monitored α value [36]. The first derivative of the double logarithmic plot d{ln{-ln[1-α(*t*)]}}/d(ln*t*) against α effectively can gives the local Avrami parameter which will be in this case labeled as n_{Local}, with an α, and this approach is seems to be a much more sensitive. Such a plot allows a more detailed evaluation of the experimentally estimated data and can emphasize the changes in the reaction kinetics during the decomposition process.

For more complex solid (or 'pseudo' solid) state reactions, the simple practice of guessing the reaction order (*n*) is not applicable and a more general method must be used to find the reaction mechanism. Many solid-state reactions take place in three stages, which may be described as follows: (*i*) the induction – formation of reaction sites or nuclei, (*ii*) the acceleration – the reaction interface increasing, and (*iii*) the deceleration – reaction interface decaying. It is expected that the solid-state reactions will follow a large variety of kinetic equations. In fact, the apparent occurrence of simple "order" equations is mainly coincidental. Many expressions have been derived in order to reflect the nature of various reaction types. These reaction mechanisms can be conveniently recognized from the experimental data using the reduced time plot method [35]. The selection of $g(\alpha)$ function is based on the shape of a reduced time plot which best describes the experimental data. By calculating values of α for selected various kinetic equations and plotting them against $t/t_{0.50}$ (where $t_{0.50}$ represents the reaction's half-life (the time value for 50 % conversion)). Theoretical predicted reacted fractions, α, *versus* $t/t_{0.50}$, for the various reaction equations, against the experimental data at

all considered operating temperatures allows us to make a selection of the best kinetic model, which is adequate to describe the investigated decomposition process. The iso-kinetic data from a number of the experimental runs should line on a single curve. This curve can then be compared to that expected for any one of a number of the different theoretical rate equations. Rate equations can be divided into three general groups: *i*) the phase boundary reactions including and the first-order reaction, *ii*) the diffusion-controlled reactions, and *iii*) the Avrami-Erofeev equations [35].

The impingement factor δ_i can be calculated from the relation [37]:

$$1-\alpha_p = \left(\frac{\delta_i}{\delta_i + 1} \right)^{\delta_i}. \tag{11}$$

The impingement factor δ_i can be calculated using the iteration method of the Eq. (11) using the experimental values of α_p. The impingement factor values can be calculated at every considered operating temperature, with the current values of α_p. It should be noted that the Avrami's (or Johnson-Mehl-Avrami) theory fails if the non-random nucleation and overgrowth processes occur. In such a case, the current approach can be modified by the introduction of the phenomenological parameter, and such parameter represents the impingement factor. The impingement factor may be correlated with the reacted fraction through the expression [38]:

$$\alpha(t) = \left\{ 1-\left[1-\delta_i (1-\alpha) \right]^{\frac{1}{\delta_i}} \right\} = \left\{ 1-P(t) \right\}, \tag{12}$$

where (1-α) is the un-reacted fraction, while $P(t)$ represents the probability that the corresponding domain (Δ_{T,R^*}) as a circle of radius R^*, is empty of nucleation centers. This probability may be evaluated through the terms of *N*-particle distribution functions or *N*-particle correlation functions [38]. Eq. (12) can successfully used for describing the instantaneous growth. In order to obtain the corresponding values for $\alpha(t)$, the δ_i values must be known and they can be found from Eq. (11). The description of the kinetics appears to be better with introducing the correlation parameter η^* which is directly connected with the impingement factor, through the relation $\delta_i \sqcup 1.340 \cdot \eta^{*-0.047}$. The description of the kinetics appears to be better for a larger value of η^*. However, the above-stated correlation between δ_i and η^* represents the weak dependence on η^*. In practice, in this interval the impingement factor can be considered constant provided the kinetics which is expressed in the dimensionless variables. Afterwards, the Avrami's curve can be recovered only for the limited case when $\eta^* \to \infty$.

3.1 Estimation of the experimental distribution of the apparent activation energies

The model of apparent activation energy distribution can acknowledge the complex nature of pyrolysis. The specific mathematical approach may provide the possible decomposition pathways of actual biomass constituents which occur during entire pyrolysis transformation. In model of reactivity distribution, the Gaussian distribution of E_a's is the most commonly used [39-41]. However, this assumption may be questionable when E_a values are widely distributed, in which case the pre-exponential factors do not necessarily remain the constant. In accordance with Miura and Maki [42] approach, this is why that the initial stated distribution does not hold the assumption about the exact form, so that the moments of the distribution are unknown. Considering that the complexity of the process is such that a continuous distribution of E_a values is assumed, and where the set of reactions (where it does not imply that obeys only to the first-order reactions) which occur with E_a values lie between E_a and E_a + dE_a at a given time t, the experimental density distribution function (*ddf*) can be obtained by differentiation of $\alpha(E_a)$ function with respect to E_a:

$$f\left(E_a\right)_{\exp} = \frac{d\left[\alpha\left(E_a\right)\right]}{d\left(E_a\right)}, \tag{13}$$

where the term $\alpha(E_a)$ (Eq. (13)) relates the total conversion with the apparent activation energy, and this can be calculated from the experimental data of α *versus* t [$\alpha = \alpha(t)$]. The following expression in a form:

$$\int_{E_a}^{E_a+\Delta E_a} f\left(E_a\right)_{\exp} dE_a, \tag{14}$$

describes the frequency or the probability that the particles within a tested sample have an apparent activation energy in the range of E_a to $E_a + \Delta E_a$.

Accordingly, the distribution satisfies the condition that $\int_{-\infty}^{+\infty} f\left(E_a\right)_{\exp} dE_a = 1$. The Arrhenius parameters are calculated for each conversion at the different operating temperatures.

The experimental density distribution function has a certain "statistical" defined form, which belongs to a category of present continuous distribution function. The distribution is characterized by specific distribution parameters, which have such characteristics that physically can describe some phenomena that occur during pyrolysis process.

The current distribution does not have to be assumed that it has the form of Gaussian distribution, therefore, it is possible to build up more complicated distribution(s) by assuming that the products of pyrolysis can be produced from more than one type of the specific reaction.

4 Results and discussion

4.1 Proximate/ultimate results

The results of proximate and ultimate analyses of the raw corn stover samples are presented in Table 1. The higher heating value (HHV) is also presented in Table 1.

Table 1. The proximate and elemental analysis of the raw corn stover samples.

Chemical composition			
Proximate analysis		**Ultimate composition[b] and higher heating value**	
Moisture (%)	5.66 ± 0.14	Carbon, C (%)	42.33 ± 1.91
Fixed carbon (%)[a]	10.32 ± 1.65	Hydrogen, H (%)	6.71 ± 0.32
Volatile matter (%)[a]	76.15 ± 1.45	Nitrogen, N (%)	0.73 ± 0.12
		Sulfur, S (%)	0.30 ± 0.02
Ash (%)[a]	7.87 ± 0.29	Oxygen, O (%)	49.93 ± 1.55
		HHV (MJ kg^{-1})	17.31 ± 0.25

[a] Dry basis.

[b] Dry ash free basis.

From Table 1, we can see that the tested samples consists approximately 76 % volatile combustible matter, while the fixed carbon content amounts to almost 10.5 %. These constituents are partitioned into the product gas, the liquid, and the solid during the onset of the various pyrolysis reactions. The obtained values were comparable to the results estimated by Zabaniotou and Ioannidou [43] and also with the United States of America Department of Agriculture (USDA) experimental data [44].

The experimentally determined higher heating value (Table 1) is somewhat lower than in the case of as-received corn stover prepared for the microwave pyrolysis (18.20 MJ kg^{-1}), but similar to rapeseed straw (17.64 MJ kg^{-1}) [45].

Comparing the experimentally obtained value for HHV (17.31 MJ kg^{-1}) with the value of HHV which was calculated on the basis of Demirbas [46] proposed formulas for HHV calculation from the proximate and the ultimate data (16.14 MJ kg^{-1} and 15.93 MJ kg^{-1},

respectively), we can notice a slight difference among the observed values. We can identify that the estimates of HHV based on the proximate data better predict the experimental HHV.

In addition, the intrinsic moisture (the moisture content of material without the influence of weather effects) is monitored. The last-mentioned concerns under the laboratory conditions.

Other factors aside, such as conversion to alcohol or gas/oil, the relationship between biomass moisture content and appropriate bio-conversion technology is essentially straight-forward, in that the thermal conversion requires low moisture content (below 50.0 %), while bioconversion can utilize the high moisture feedstock samples.

However, it should be noted that thermal conversion processing can also use feedstock with high moisture content but the overall energy balance for conversion process is adversely impacted. The result of the moisture content (Table 1) meets all the requirements for biomass feedstock moisture contents which are necessary for the successful implementation of the laboratory pyrolysis experiments.

The carbon content of tested corn stover sample was in the range of 42.0-43.0 % (Table 1) which is typical for herbaceous biomass feedstocks [47]. Oxygen content (49.93 %) (Table 1) is in agreement with actual calculations outlined in European Standard EN 15296.

Namely, in a general manner, the ultimate composition including primarily the carbon, hydrogen, nitrogen, and the oxygen contents can be correlated to the cellulosic feedstock materials, such as the corn stover, cobs or wood. Actually, the chemical composition of the corn stover, the wheat straw and the switchgrass, is relatively similar when harvested to maximize the lignocellulosic component.

It should be noted that when grown in the different environments, considerable variation in feedstock composition may occur. On the other hand, it should also be noted that the corn stover to the grain ratios are about 1:1 on a dry matter basis, where the corn stover contains about 38 % cellulose, 26 % hemicelluloses and 19 % lignin, and 5 % of crude proteins [48].

The liquid product, bio-oil, approximates the biomass in elemental composition. Bio-oil is composed of a very complex mixture of oxygenated hydrocarbons, reflecting the oxygen contents of feedstock sample (Table 1).

4.2 Static pyrolyis curves and conversion fraction profiles

Fig. 1 (a)-(b) shows the experimentally obtained static thermogravimetric curves of corn stover pyrolysis at operating temperatures of T = 180, 230 and 270 ºC, as well as the appropriate conversion (integrated kinetic) curves, observed at the same operating temperatures, respectively.

Based on thermogravimetric (TG) measurements (Fig. 1 (a)), we can see that with the varying the operating temperature, there is some variation in the residual mass loss Δm_{res}, wherein the following values of Δm_{res} were obtained: $\Delta m_{res}^{180\ °C}$ = 28.50 %, $\Delta m_{res}^{230\ °C}$ = 35.00 % and $\Delta m_{res}^{270\ °C}$ = 60.00 %, respectively.

It is obvious that the total mass loss in the corn stover biomass under the pyrolysis conditions significantly depends on the applied interval of the operating temperatures which was used for the measurements.

All measured thermo-analytical (TA) curves (Fig. 1 (a)) are correctly shifted to the lower range of the pyrolysis time durations with an increasing of the applied operating temperature, which is a genuine indication of the thermally-activated heterogeneous process, confirming the validity of the completed TA measurements.

However, the distance between the observed thermogravimetric curves at the actual operating temperatures is not the same, and also the shape of the TG curve at 180 ºC does not match the shapes of the curves at the other applied operating temperatures (see Fig. 1 (a)), which preliminarily may indicate a change in the reaction mechanism of the pyrolysis process or in the change of the rate-determining step.

This uneven spacing between thermo-analytical curves (keeping in mind the rather small sample weight used in the experiments and elimination/blocking of the diffusion-mass transfers) may indicate a “kinetic asymmetry” of the current pyrolysis process, which clearly, in this preliminary phase of the study, provides identification of a fairly complex process that can involve several reaction stages.

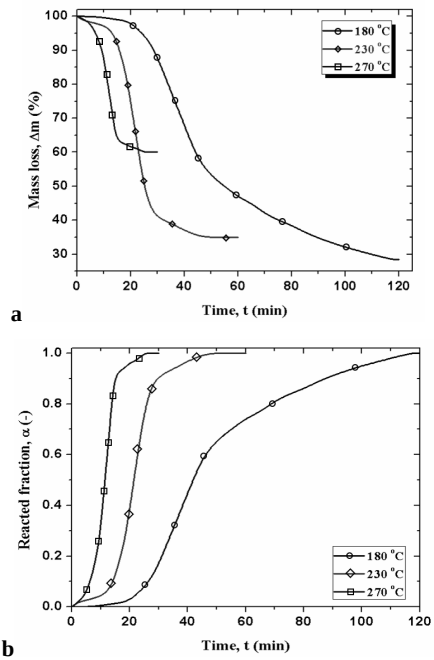

Figure 1. (a)-(b). Experimentally obtained static thermogravimetric curves of corn stover pyrolysis process at operating temperatures of T = 180, 230 and 270 °C, and the appropriate conversion (α – t) curves at the same observed operating temperatures, respectively.

If we look at the overall flow of the TG curves at a given operating temperatures, we can notice that there are three characteristic segments in the mass loss of the sample (Fig. 1 (a)). In the first five minutes of the process (looking at almost all operating temperatures) we have the loss of water and eventually light volatile compounds in the tested biomass sample [49]. The low moisture content (Table 1) in the investigated corn stoves samples resulted in the low mass loss during actual stage of the mass loss behaviors.

After this, first stage, there was negligible mass loss (about 0.32 % considering, for example, the TG curve at 180 °C) in time duration period of 5 – 10 minutes, which may indicates on the decomposition reactions related to the residual light volatile compounds in a series. The second phase of mass loss which starts at about 10 - 15 minutes and where ends at 45 minute at 180 °C, then at 25 minute at 230 °C, and finally at 17 minute at 270 °C, represents the main (active) pyrolysis zone and which involves the decomposition of the hemicelluloses and cellulose pseudo-components of corn stover. The slow decomposition of

the lignin pseudo-component represents the third phase of mass loss (for 180 ^{o}C, this term corresponds to the pyrolysis time duration above 45 minute) and this means a passive (accessary) pyrolysis zone. This behavior is typical for all lignocellulosic materials [50]. Variation of above-mentioned pseudo-components across biomass sample may causes different responses to pyrolytic treatment. We can expect that the main process step is in fact the decomposition of cellulose, since the cellulose is the dominant component in the corn stover biomass material.

However, it should be noted that the inclination of the part of the TG curve which corresponds to the last phase in the pyrolysis process at the operating temperatures of 230 and 270 ^{o}C is different from the inclination of part of the TG curve at the lowest operating temperature (Fig. 1 (a)). The parts of the TG curves at the aforementioned operating temperatures are quite steep and not decline so mild as in the case of TG curve at 180 ^{o}C for the same observed segment (Fig. 1 (a)). This phenomenon may indicates that at the higher operating temperatures (> 230 ^{o}C) in the process stage which corresponds to the lignin decomposition can reach an additional complexity in terms of pyrolysis kinetic mechanism, as opposed to the same terms related to the lowest operating temperature. The saturation parts in all recorded static TG curves correspond to the ash formed and the presence of the fixed carbon (Fig. 1 (a)). The conversion (integral) curves of the actual process (Fig. 1 (b)) show characteristic acceleratory behaviors at all observed operating temperatures. It can be observed that with an increasing of operating temperature, the duration of the induced time (t_{ind}) period is shortened. The shapes of these curves are typical for processes which include the nucleation and growth reaction steps of the formed product phase, which incorporate the significant temperature dependency on the reaction rate. It may assumes the existence of the autocatalytic mechanism with a more or less important role of the precipitated phase on overall kinetics, and where the identified transformation can be described by the fractal parameters, which have the same statistical character as the whole.

4.3 Isoconversional reaction profile

Fig. 2 shows isoconversional reaction profiles obtained from integral and differential (Friedman's) "model-free" approaches. Corresponding errors in calculation of E_a values were presented in a form of error bars, along Y-axis. From Fig. 2 we may see that values of apparent activation energy (E_a) vary with α during the pyrolysis.

It can be observed that at the very beginning of the process, including transformations inside the system up to $\alpha = 0.20$ [20 %], a decrease in the value of E_a from 37.3 to 29.0 kJ mol^{-1} (considering results estimated using the Friedman's method) may corresponds to evaporation of residual water and vapors with a production of some non-condensable gases [51]. It should be noted that a large part of produced vapors can be condensed to a brown liquid bio-oil, leaving the non-condensable gases as a combustible fuel for the immediate use. After $\alpha = 0.20$ (taking into account both isoconversional approaches), we can identify a fairly wide range of conversion, which includes central part of the pyrolytic process within 0.20 [20 %] $\leq \alpha \leq$ 0.60 [60 %], where the E_a value is almost the constant.

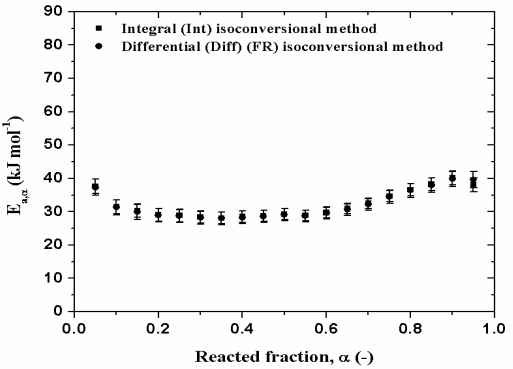

Figure 2. Isoconversional reaction profiles obtained from integral and differential (Friedman's) "model-free" approaches, for the static pyrolysis process of corn stover.

The following average values of E_a in the interval of $0.20 \leq \alpha \leq 0.60$ were obtained and they are as follows: $\langle E_a \rangle_{Int}$ = 28.9 ± 1.7 kJ mol^{-1} and $\langle E_a \rangle_{FR}$ = 28.7 ± 1.9 kJ mol^{-1} estimated by integral and differential (Friedman's) isoconversional methods, respectively. The obtained values of E_a calculated by the integral and differential "model-free" approaches are very similar, indicating that the current part of the pyrolysis process can be described by the single-step reaction model. Beyond 60 % of conversions, we can notice an increase in the value of the apparent activation energy, from 29.6 up to 39.9 kJ mol^{-1}. This part of the pyrolysis process can be attributed to the formation of bio-char and in saturation of the fixed carbon elements. This behavior in E_a is specific for the slow pyrolysis, which is focused on bio-char production, and is characterized by applying the lower operating temperatures (below 400 ^{o}C). In this case, biomass components undergo complete deconstruction by the

loss of pendant groups on rings and chains, and also the depolymerization and fragmentation of its three main component polymers. The slow pyrolysis approximately equal amounts of bio-oil and light gases. The solid product yields at the lower operating temperatures (as applied in the operating temperature range in actual experiments) amount about 30 – 36 % in accordance with Bridgwater [52].

In comparison with coal structure, the polymers of the hemicelluloses, cellulose and lignin which constitute macromolecular structure of biomass and other woody materials are linked together by relatively weak bonds (in respect to those present in coal) with a bond energy of about 380 – 420 kJ mol^{-1} [53]. However, it is important to note that these bonds are less resistant to the heat when exposed to the low/lower operating temperatures. This clearly leads to a drop in the values of the apparent activation energy, and if we make a comparison with a coal. In this regard, the values of E_a, and in particular those for $\alpha = 0.20 – 0.60$ for a selected thermo-analytical regime of the pyrolysis, are in good agreement with E_a range as reported in the literature [54,55]. Based on the calculated value of E_a in the conversion range where the apparent activation energy shows almost constant behavior (which is one link in the kinetic triplet), we may refer for the further examination of the possible occurrence of the reactivity differences among the pseudo-components within the studied biomass sample.

4.4 Investigation of reaction mechanism of pyrolysis process

The reduced time plot method was used for a preliminary assessment of the reaction mechanism in the case of studied pyrolysis process.

Fig. 3 shows the theoretically constructed reduced time plots (full line curves) with a various solid-state mechanism models [56] (which comprises the phase boundary controlled reactions, R2 (contracting area), R3 (contracting volume), random nucleation with one nucleus on the individual particle – F1, nucleation and growth models – Am (m = 1.5, 2, 3, and 4), and diffusion controlled reactions (one-D1, two-D2, and three-D3 (Jander equation), D4 (Ginstling-Brounshtein equation) diffusions)), and experimental ones (symbol curves) obtained at the different operating temperatures (T = 180, 230 and 270 ^oC). We can notice that with the variation of the operating temperature, the experimental points follow different pyrolytic reaction mechanisms.

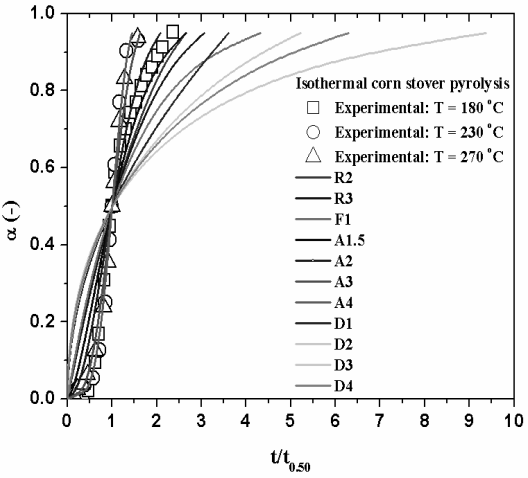

Figure 3. Theoretically constructed reduced time plots (full line curves) with a various solid-state mechanism models, and the experimental ones (symbol curves) obtained at the different operating temperatures (T = 180, 230 and 270 °C), for the static pyrolysis of corn stover.

At lowest operating temperature (180 °C), and at the lower α values, the experimental data follow A4 reaction mechanism, while at higher α values (beyond 50 % of conversions), the data lie between A1.5 and A2 theoretical reduced time curves, attached to the Avrami's nucleation and growth models. At higher operating temperatures (230 and 270 °C), in the entire conversion range, the experimental data lie on/around the theoretical reduced time curve for A4 kinetic model. The "retardation" period was greatly shortened at 270 °C, where higher temerature is able to vaporize fragments of the longer chains which also result in a faster decomposition, thus leading to the reduction in the "retardation" period.

In order to check whether the pyrolytic process obeys nucleation and growth type of reaction models (Am), the two special functions (Y(α) and Z(α), normalized within [0,1]) were applied. Fig. 4 shows normalized Y(α) and Z(α) functions at various operating temperatures for the static pyrolysis process of corn stover samples.

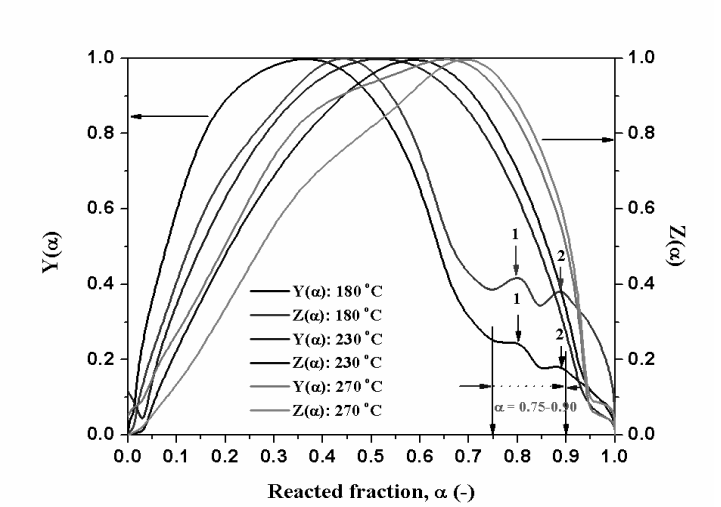

Figure 4. The normalized $Y(\alpha)$ and $Z(\alpha)$ [0,1] functions at the various operating temperatures for the static pyrolysis process of corn stover.

From Fig. 4 we can see that $Y(\alpha)$ and $Z(\alpha)$ functions show the strong sensitivity to an changing of the operating temperature, while showing more than one peak. Complex behavior is particularly pronounced at T = 180 °C, where both functions, in the conversion range of α = 0.75 - 0.90, show two peak values (designated by "1" and "2", respectively). Their shapes are different from the shape of the functions $Y(\alpha)$ and $Z(\alpha)$ at the operating temperatures of 230 and 270 °C (Fig. 4). In addition to the main peak which appears up to α = 0.50, two additional peaks at 180 °C occurring in the conversion range, where E_a value increases with α (Fig. 2). This behavior can be attributed to the heterogeneous composition of the corn stover, where the pyrolysis is a complex process involving consecutive and parallel thermal decomposition reactions. Namely, if we give attention on three main pseudo-components, up to 220 °C pyrolysis principally affects hemicelluloses, and a single apparent kinetic model can be probably obtained. At increasing operating temperature, the cellulose decomposition becomes more significant giving a more complex pyrolysis mechanism pathways, but the difference in the levels of reactivity between these two pseudo-components is still unknown. However, the cellulose decomposition reaction would be significantly affected by the resistance to the mass and heat transfer in particles. The lignin decomposition is a slower and comprises the broader operating temperature range (200 – 500 °C) than the cellulose and hemicelluloses pseudo-components. Thermal decomposition of lignin is generally influenced by the heat and mass

transfer processes, which significantly affect apparent activation energy and pre-exponential factor for its decomposition. The behavior of $Y(\alpha)$ and $Z(\alpha)$ functions with the change of the operating temperature clearly indicates the complex pyrolysis reactions, whereby still do not have a clearly defined picture of the most probable kinetics model that can comprehensively describe the pyrolytic process. Table 2 shows the values of parameters α_M, α_p^{∞} and α_p attached to $Y(\alpha)$ and $Z(\alpha)$ functions, as well as for rate-time curves correlated with pyrolysis.

Table 2. The values of parameters α_M, α_p^{∞} and α_p at the different operating temperatures (180, 230 and 270 °C), for pyrolysis process of the corn stover.

Operating temperature, T (°C)	α_M	α_p^{∞}	α_p
180	0.364 ± 0.003	0.442 ± 0.004	0.442 ± 0.004
230	0.519 ± 0.005	0.589 ± 0.005	0.589 ± 0.005
270	0.661 ± 0.006	0.694 ± 0.005	0.694 ± 0.004

The resulting parameters values presented in Table 2 show increasing behavior with an increasing of the operating temperature in the α's intervals such as $0.364 \leq \alpha_M \leq 0.661$, and $0.442 \leq \alpha_p^{\infty} \leq 0.694$, respectively. For the Avrami-Erofeev models (Am) with $m > 1$, the $Y(\alpha)$ functions exhibit a maximum, whose position (α_M) depends on the value of m. However, the same property is demonstrated by the truncated Šesták-Berggren (with $Q = 0$ in the empirical three-parameter Šesták-Berggren model equation: $f(\alpha) = \alpha^M \cdot (1-\alpha)^N \cdot [-\ln(1-\alpha)]^Q$) or extended Prout-Tompkins model in a form of $f(\alpha) = \alpha^M \cdot (1-\alpha)^N$ [57] which is an example of an autocatalytic model. At all operating temperatures, the maximums of $Y(\alpha)$ functions lie within $0 < \alpha_M < \alpha_p$ interval, while the values of α_p^{∞} at T = 180 and 230 °C (Table 2) are below the value of $\alpha_p^{\infty} = 0.632$ which is characteristic "finger-print" value attached to Avrami-Erofeev kinetic models. At the highest operating temperature, the α_p^{∞} is equal to 0.694 which most closely corresponds to the value of α_p^{∞} (0.704) attached to contracting (sphere) volume kinetic model [58].

Results show the mixing pyrolysis mechanism which probably involves the combination of autocatalytic reactions with changing in the reaction geometry. In order to verify any changes in the rate-determining steps during studied process, the Avrami's double logarithmic (*ln—ln*) plots method was performed at all observed operating temperatures. Fig. 5 shows Avrami *ln—ln* plots at different operating temperatures for pyrolysis process at observable reacted fraction regions. From presented plots, we can notice that at all operating temperatures, there is a clear separation of experimental points in two reaction stages with

appropriate changes in conversion ranges, which are marked with "I" and "II", respectively. At the same figure, the corresponding values of Adj. R-Square (R^2) are also presented.

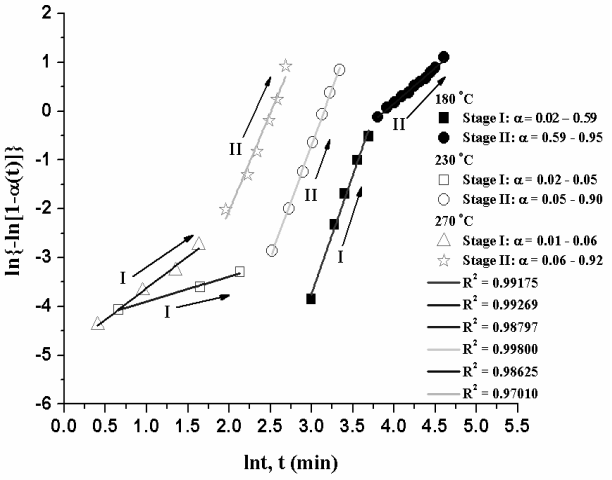

Figure 5. The Avrami's *ln—ln* plots at the different operating temperatures (T = 180, 230 and 270 °C), for static pyrolysis process of corn stover at the observable reacted fraction regions.

It can be seen from Fig. 5, that the linear plots related to identify process stages are differ significantly in slopes. The reaction stages duration (in respect to α's longevity) differ significantly with changing of the operating temperature. This is especially true in the first process stage ("I") at the higher operating temperatures (230 and 270 °C). At the lowest operating temperature (180 °C) (where α range is wide, within the first process stage), the higher slope may indicate the higher reactivity of hemicelluloses compared to reactivity of cellulose. With an increasing of operating temperature ($T \geq 230$ °C), the longevity of the first process stage is drastically shortening, where the lower slopes are consistent with a lower hemicelluloses' reactivity compared to that of cellulose. In that case, the first linear plots become shorter as T increases, because the more hemicelluloses decompose during the pre-heating stage. At $T \geq 230$ °C, the second linear plots are longer than the one at T = 180 °C (covering a wider α range) where the hemicelluloses completion is achieved, including clearly obtained straight lines corresponding basically to the cellulose decomposition. However, it should be noted that during the dominance of cellulose decomposition, in a substantial increase in temperature, the contribution of lignin decomposition can also become quite

noticeable. Table 3 lists Avrami's parameters values such as overall rate constant (k) and kinetic exponent (m), in corresponding process stages limited to observable reacted fraction ranges ($\Delta\alpha$) at various operating temperatures.

Table 3. The Avrami's parameters evaluated for the static pyrolysis process of the corn stover.

T (°C)	Stage	$\Delta\alpha$[a]	$m\ln(k)$	$\ln(k)$	k (min^{-1})	m	RSS[b]
180	I	0.02 – 0.59	-18.28819 ± 0.75014	-3.77076	0.02303	4.85 ± 0.22	0.04178
	II	0.59 – 0.95	-5.66891 ± 0.16739	-3.88281	0.02059	1.46 ± 0.04	0.00901
230	I	0.02 – 0.05	-4.40796 ± 0.06356	-8.64306	0.00018	0.51 ± 0.04	0.00178
	II	0.05 – 0.90	-14.54620 ± 0.25211	-3.14853	0.04291	4.62 ± 0.08	0.01763
270	I	0.01 – 0.06	-4.91608 ± 0.10358	-3.81091	0.02213	1.29 ± 0.09	0.01310
	II	0.06 – 0.92	-10.04293 ± 0.74912	-2.51073	0.08121	4.00 ± 0.31	0.13667

[a] Reacted fraction range.

[b] Residual sum of squares.

From Table 3, we can see that there is great variation in the m exponent with changing of the operating temperature, going after the process stages. With an increasing of operating temperature, within the first process stage, the reactivity of hemicelluloses decreases (which indicates the parameter m, which drops from 4.85 up to 0.51 (Table 3)). On the other hand, at elevated operating temperatures, the cellulose reactivity dominates including the significant lignin contributions, where the parameter m increases from 1.46 up to 4.62 (the second process stage). From bulk mechanism standpoints, the decomposition process probably can start from cellulose amorphous domains from entire sample. When crystalline domains decomposition takes place the decomposition initially occurs on the crystallites surface and phase boundary-controlled reactions. The relatively low values of E_a which were observed, might be also attributed to thermal decomposition of the tested sample, which was controlled by the dehydration process resulting in anhydrocellulose. However, it should be noted that, if necessary, more water retained in the cellulose structure may be responsible for initiate decomposition process by dehydration which probably results in lower E_a values.

Fig. 6 shows variation of local Avrami parameter (n_{Local}) values with α changing, which corresponds to all identified process stages at the various operating temperatures.

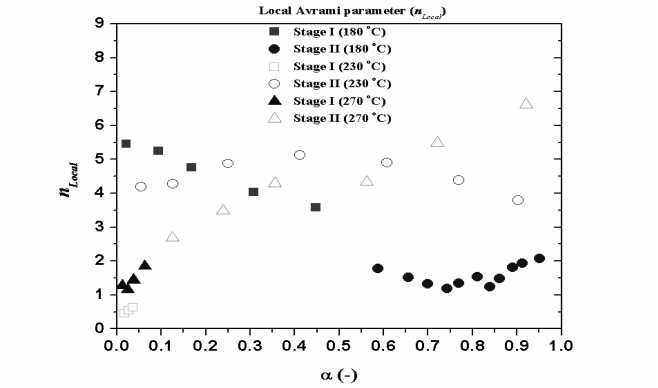

Figure 6. The variation of the local Avrami parameter (n_{Local}) values with α changing, which corresponds to the identified process stages at the various operating temperatures, for the studied pyrolysis process.

It can be observed from Fig. 6 that the n_{Local} data are distributed in a variety of α intervals and show drastically different values, within identified stages. These variations indicate that the pyrolysis process can not be described through a simple single-step reaction model, where multi-steps decomposition exists. The obtained values of n_{Local} are similar to the values of *m* exponent, estimated from the Avrami *ln—ln* plots. To describe the pyrolysis process more precisely and to distinguish which one of the several kinetic models can be used for actual process, we must realistically check whether the Avrami-Erofeev kinetic model really exists or represents the *artificial* model.

The parameter *m* can be correlated with α_M value through relation $m = 1/[1 + \ln(1-\alpha_M)]$, and based on position of the main peak of $Y(\alpha)$ function, the corresponding value of *m* can be calculated. Table 4 lists the values of *m* which were calculated on the basis of above-stated relation, and also values of δ_i and η^* at different operating temperatures (180, 230 and 270 °C).

Table 4. Values of the m exponent (calculated from the equation $m = 1/[1 + \ln(1-\alpha_M)]$) and the values of the impingement factor (δ_i) and the correlation parameter (η^*), at various operating temperatures (180, 230 and 270 °C).

Operating temperature, T (°C)	m	δ_i	η^*
180	1.83	0.586	4.392×10^{7}
230	3.73	3.588	7.925×10^{-10}
270	-12.23	-	-

From Table 4, we may see that at the operating temperatures of 180 and 230 °C, the parameter m corresponds to $m \approx 2$ and $m \approx 4$, respectively, and actual results indicate on transition mechanism from one-dimensional growth (i.e., the fibrilar growth with nucleation-controlled process) and the "instantaneous nucleation" attached to structures of the self-assembled fibrillar networks (which are characteristic for crystalline fibrils of the cellulose that are linked together by the less-ordered polysaccharides (such as hemicelluloses) and embedded in lignin) to the interface controlled growth ($m \sim 4$) and constant nucleation rate. Therefore, the resulting value of the parameter m above the 4.00 that are shown in Table 3 as well as the high values of the local Avrami parameter from I — II crossing behaviors (Fig. 6), clearly indicate transient nucleation implying negative deviation from some universal value. This is an authentic result obtained by studying the static pyrolysis process of corn stover within operating temperature range of ΔT = 180 – 270 °C. Namely, this is especially expressed at elevated operating temperature, such as 270 °C, where we get a negative value of the parameter m (Table 4). At the present, when we have a combination of above-mentioned factors, then it becomes difficult to predict a nucleation mechanism from the m exponent. In fact, this assumption is also confirmed on the basis of the results shown in Table 4 and associated with δ_i and η^* terms. At the lowest operating temperature (Table 4), we can see that the impingement factor (δ_i) is low (0.586) and correlation parameter (η^*) is quite high (4.392×10^7 and can be approximated to $\eta^* \rightarrow \infty$). Only in the observed case, the Avrami-Erofeev kinetic model can be applied in a true sense, while in the other cases (Table 4) it becomes "*artificial*". At T > 180 °C, the considered kinetic model is not valid for mechanistic description of the pyrolysis process. Therefore, it is necessary to find a "general" (*flexible*) kinetic model, which may describe the pyrolytic behavior of the studied system in the entire operating temperature range. This model actually represents the accommodation function which can "*measure*" the discrepancy of idealized $f(\alpha)$ model from the actual kinetic model function. The new introduced function should reduce the difference between of idealized $f(\alpha)$ from the practical process.

For static data, the simple test approach for checking whether the reaction rate is at its maximum value as soon as the sample reaches the static operating temperature is the establishment of dependency $\ln(d\alpha/dt)$ *versus* $\ln(1-\alpha)$.

If the plot is linear for times after the sample is truly static, the reaction mechanism obeys the first-order kinetics or the nearly so. If the plot is concave downward, the reaction mechanism is likely to be a contracting volume (such as R2 and R3 models). If the plot is concave upward, the reaction mechanism probably has a increasing diffusion resistance. In observed cases, the process is deceleratory, and the deceleratory model must be used.

Fig. 7 (a) shows the plots of $\ln(d\alpha/dt)$ against $\ln(1-\alpha)$ at the different operating temperatures, for the static pyrolysis process of corn stover samples.

It can be seen from Fig. 7 (a) that at T = 180 ^{o}C, in an earlier stage of the process, we have a typical concave downward $\ln(d\alpha/dt)$ *vs*. $\ln(1-\alpha)$ plot, while in the later stage, the observed plot shows the almost linearly behavior. On the other hand, at 230 and 270 ^{o}C, there are typical concave downward $\ln(d\alpha/dt)$ *vs*. $\ln(1-\alpha)$ plots, in the entire conversion ranges.

With regard to these results, we can conclude that the contracting volume-controlled process exist, with the presence of reaction model which includes the kinetic controlling parameter. This parameter may be associated with nucleation density on the reaction surface and with a degree of strain at the phase boundary. Changes in nucleation density may leads to different reactivities at the reaction interfaces and thus to different rate behaviors (Table 3). In this regard, it appears that the reaction geometry of the overall process cannot be expressed in terms of an integral value of reaction-order parameter. Bearing in mind the resulting sigmoidal (acceleratory) shapes of the experimental conversion curves (Fig. 1 (b)) then, the reaction rate is not at its maximum value when the sample reaches the static conditions, and in the actual case the process possessed the acceleratory nature. If the tested process at the various operating temperatures has the potential reaction peak (as shown in the experimental rate-time curves in Fig. 7 (b)), an Avrami-Erofeev models (which here are disabled) or the truncated Šesták-Berggren model are the appropriate.

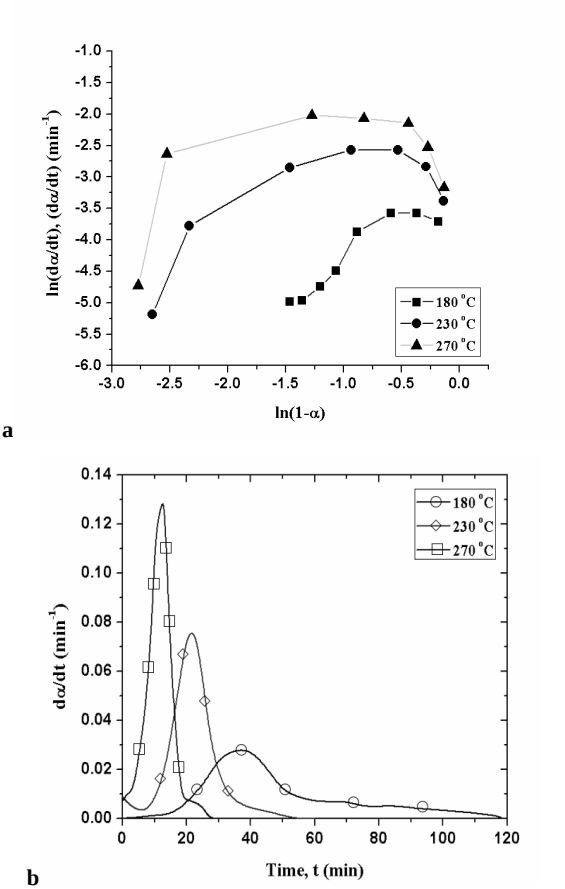

Figure 7. (a)-(b). The plots of ln(dα/d*t*) against ln(1-α) at the different operating temperatures, for the static pyrolysis process of corn stover and experimental pyrolysis rate (dα/d*t* – *t*) curves.

If we take into consideration all the above facts, in order to eliminate disagreement between the idealized process assumed in formulating the kinetic functions and the actual process under the investigation (becuase this disagreement leads to some distortion of the Arrhenius parameters), the two-parameter Šesták-Berggren (SB) model was used.

According to the SB model, the following equation:

$$\ln\left[\left(\frac{d\alpha}{dt}\right)\cdot\exp\left(\frac{E_a}{RT}\right)\right]=\ln A+N\ln\left[\alpha^{P}\cdot(1-\alpha)\right] \tag{15}$$

is the valid. From the linear relationship represented by Eq. (15), the SB kinetic exponent N (which "N" refers to the reaction order), and the pre-exponential factor (A) can be calculated from the slope and the intercept of the estimated plots, at the various operating temperatures.

The value of the second SB exponent M can be derived from $M = P \cdot N$ and $P = \alpha_M/(1-\alpha_M)$. Value of P is connected to the maximum value of $Y(\alpha)$ function. The above relation is valid for conversion range of $\alpha = 0.20 - 0.80$, where for calculation procedure, the apparent activation energy (E_a) value calculated from differential isoconversional method was used.

The results which were obtained on the basis of the fine fitting of the dependence $\ln[(d\alpha/dt)\cdot\exp(E_a/RT)]$ *versus* $\ln[\alpha^P\cdot(1-\alpha)]$ are presented in Table 5.

Table 5. The calculated SB kinetic parameters M, N, and A for the static pyrolysis of corn stover samples. The same table also presents the values of objective function, Ω, and deviations (*Dev* in %) between the observed and calculated rate-time ($d\alpha/dt$ — t) curves, at the various operating temperatures evaluated from the non-linear least-square analysis (using the actual kinetic triplet)

T (°C)	P	ln$A$	A (min^{-1})	M	N	Ω	*Dev* (%)
180	0.572	6.92915 ± 0.34789	1.022×10^3	1.565	2.736 ± 0.263	2.180×10^{-4}	2.300
230	1.079	5.71575 ± 0.12592	3.036×10^2	1.008	0.934 ± 0.077	2.259×10^{-5}	0.860
270	1.950	5.17464 ± 0.19180	1.767×10^2	0.801	0.411 ± 0.080	1.068×10^{-4}	1.080
Average	1.200	5.93985 ± 0.22187	5.010×10^2	1.125	1.360 ± 0.140	1.160×10^{-4}	1.413

From the results listed in Table 5, we may see that with an increasing of operating temperature, both parameters (M and N) decrease, while the pre-exponential factor (A) remains very low (with magnitude of $\times 10^2$ min^{-1}).

The low values of A (Table 5) are typical for appearance of the surface reactions. It has been shown [33] that increasing value of the exponent M indicates a more important role of precipitated phase on the overall kinetics. On the other hand, the higher value of N ($N > 1$) indicates increasing reaction complexity.

In accordance with above facts, with an increasing of operating temperature, the complexity of the process is reduced, and can be observed the less impact of the precipitated phase.

However, it should be noted that at the lowest operating temperature (180 °C), the exponent M (1.565) does not equal to the zero and N (2.736) is the apparently larger than M (Table 5), therefore, this phenomenon suggests that the autocatalytic and the non-autocatalytic reactions occur simultaneously.

The decline in the value of the exponent M under the unity with the increasing of the operating temperature above T = 180 °C suggests the amplifying acceleratory behavior, where the value of the exponent M = 0.801 and the very low value of N = 0.411 at T = 270 °C indicate fairly rapid surface reactions. Namely, the exponent M is related to the autocatalytic concentration of the reactive species, which is the largest at 180 °C, while at 230 °C this concentration decreases to some "intermediate" levels ($M \approx 1$ at 230 °C, Table 5). Current surface reaction geometry activities become dominant at the highest operating temperature. Actually, the kinetic parameter value N = 0.411 at the operating temperature of T = 270 °C enters into the fractal dimension constant as $\Psi \sim ½ = 0.500$ ($N = 0.411 \approx 0.500$), which corresponds to the contracting area mechanism, as it was assumed on the basis of the previous results (see above discussion). It is interesting that non-integral value of N is taken as value corresponding to fractal dimension (Ψ), although relationship between N and Ψ varies due to macroscopic character of conversion curves (Fig. 1 (b)). Above-confirmed facts are the main reason why Avrami-Erofeev model fails at the highest operating temperature (Table 4). Using data from the thermo-analytical (TA) curves, the experimental data of dα/dt rate curves are compared with the observed dα/dt rate curves, using the above-confirmed reaction mechanism kinetics. For comparison between experimentally evaluated and predicted rate-time curves, the non-linear least-square analysis was applied (Eqs. (4) and (5)). Fig. 8 shows actual comparison of tested rate-time curves.

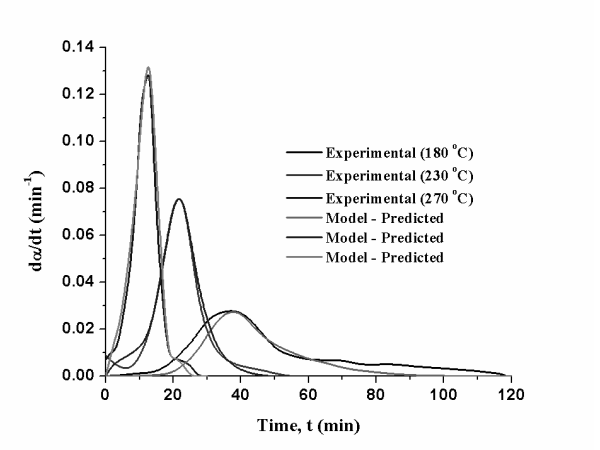

Figure 8. Comparison between experimentally evaluated, and the predicted rate-time curves, using the non-linear least-square analysis, for the static pyrolysis process of corn stover.

Fig. 8 shows that predicted curves match well with the experimental curves, although there is some deviation for static run at 180 ^{o}C, where one of the reasons may be encouraged because of the above-mentioned complexity of the process, which occur the autocatalytic and non-autocatalytic effects. In addition, under the other operating temperature values, the prediction rate-time curves are almost the same as the experimental ones, showing that the SB kinetic model very well describes static pyrolysis of the corn stover samples. Confirmation of a fairly good agreement between experimentally obtained and the modeled rate-time curves also give the values of terms such as Ω and *Dev* (%) from the non-linear least-square analysis (Table 5).

4.5 A new reactivity model for pyrolysis process of corn stover

From results presented in previous sub-section, it is need to obtain some important clues about the selection of the proper reaction models for the individual steps in the complex multi-step process mechanism. It is important to emphasize that some complex processes do not obey someone specific and regular kinetic model, but obviously include set of independent, parallel reactions whose contributions are controlled by the statistical distribution function. In this case, distributed reactivity is often introduced as a distribution of the apparent activation energies.

The initial distribution is usually unknown, but experimentally evaluated distribution of E_a's serves as a guide for getting real, theoretically derived density distribution function of process reactivity. Fig. 9 (a) shows plotting of the $\alpha(E_a)$ function for the corn stover pyrolysis under static conditions. It is observed that as conversion increases, the energy barrier that must be surpassed us higher. This is an expected result due to the sequence of the reactions during pyrolysis process, i.e. the bond breakage of the weakest functional groups to the breakage of closed molecular ring structures. Corresponding experimental density distribution function (*ddf*) of E_a values is presented in Fig. 9 (b) (the full line curve).

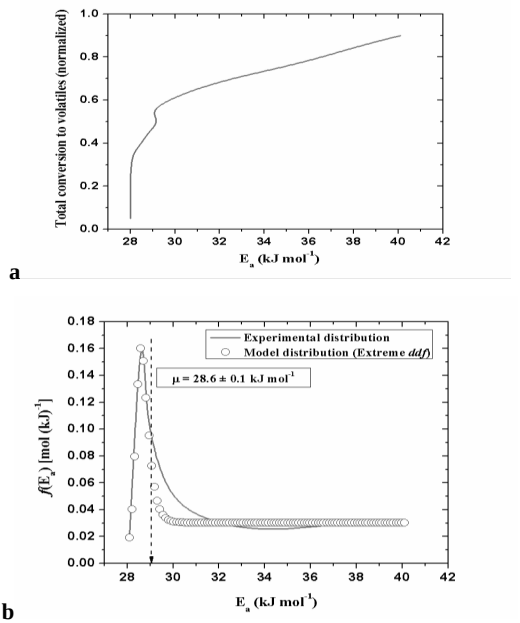

Figure 9. (a) The α(E_a) function for the corn stover pyrolysis under static conditions, **(b)** The experimentally evaluated and the model distribution (Extreme density distribution function of the apparent activation energies), for the investigated pyrolysis process. The actual mean value (μ) is marked in the same figure.

The corresponding experimental *ddf* can be adequately (through numerical procedure) fit with a statistical function in a form:

$$f\left(E_a\right)=\frac{1}{\sigma}\exp\left[\frac{\left(E_a-\mu\right)}{\sigma}\right]\cdot\exp\left\{-\exp\left[\frac{\left(E_a-\mu\right)}{\sigma}\right]\right\}, \tag{16}$$

which represents theoretically derived density distribution function and its form corresponds to *Extreme* (type I) continuous probability density function [59] of the activation energy counterparts.

The appropriate cumulative probability function ($F(E_a)$) can be expressed in a form as:

$$F\left(E_a\right)=1-\exp\left\{-\exp\left[\frac{\left(E_a-\mu\right)}{\sigma}\right]\right\}, \tag{17}$$

where μ and σ represent the mean (expected) value of the continuously distributed random variable (where the random variable is the apparent activation energy) and the standard deviation (dispersion), respectively.

In the context of reliability modeling and transferred to a complex pyrolysis process, if a tested system consists of the N^* reactions in a series, and system is decomposed when the first of these reactions suffers decomposition, then the system decomposition times are the *minimum* of N^* random component decomposition times.

Globally, this refers to the pseudo-components level in the biomass system. If the E_a values are "bounded" below the mean (where the distribution curve is more tilted to the left with a long tail towards the higher E_a values (Fig. 9 (b)) then the limiting distribution is the Weibull probability. The distribution curve is denser for smaller values of E_a (< 30 kJ mol^{-1}) which is a characteristic feature for a rapid pyrolysis process. It should be noted that the reactions having low E_a values contribute with α values near 0.50 [50 %] (Fig. 2) indicating that these reactions release an important amount of volatiles.

The mean value and dispersion for extreme distributed reactivity can be calculated based on a linear transformation *via* the double logarithmic procedure, where we get a final expression in a form:

$$\ln\left\{-\ln\left[1-F\left(E_a\right)\right]\right\} = -\frac{\mu}{\sigma} + \frac{E_a}{\sigma}, \tag{18}$$

where the slope in Eq. (18) is equal to $1/\sigma$, while the intercept is equal to $-(\mu/\sigma)$. In addition, Fig. 10 shows the linear dependency from the Eq. (18), which includes E_a values around the peak of the experimental distribution shown in Fig. 9. The dependent variable represents the apparent

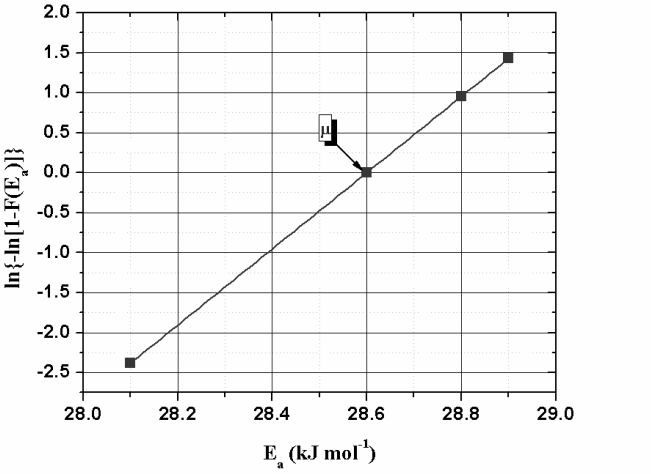

Figure 10. The linear dependency established from Eq. (20), which includes the E_a values around the peak of the experimental distribution.

From evaluated linear dependence, the following values of statistical parameters were obtained: μ = 28.6 ± 0.1 kJ mol^{-1} and σ = 0.21 ± 0.09 kJ mol^{-1}. The actual mean value (μ) is marked in Figs. 9 and 10. The obtained mean value (28.6 kJ mol^{-1}) belongs to the option that is present in the case of low apparent activation energy during biomass pyrolysis. Namely, this result suggests that E_a for high ash biomass is lower than that of low ash biomass for both raw and partially composted samples [60]. It should be noted that high ash content absorbs heat, inhibiting pyrolysis, particularly devolatilization early steps, due to endothermic character of involved reactions. Corn stover is a heterogeneous material, varying in composition and mineral concentration. Remaining residue is composed of the mineral compounds usually contains phosphorus, sodium, potassium, sulfur, and other minerals. This retention of E_a value at low level probably originates from mineral content linked to the ash, which has harmful effect on volatiles yield. Otherwise, a more energy would be available for thermal decomposition of organics.

However, the Weibull distribution and the Extreme distribution have a useful mathematical relationship. If t_1, t_2,…, t_N are a sample of random times of decompositions from the Weibull distribution, then ln(t_1), ln(t_2),…, ln(t_N) are random observations from the Extreme distribution. In other words, the natural logarithmic of a Weibull random decomposition time is an extreme value random observation.

If the Weibull distribution has the shape parameter β and the scale parameter η, then the Extreme distribution (after taking natural logarithms) has μ = ln(η) and σ = 1/β. Because of this relationship, the computer programs designed for the Extreme distribution can be used to analyze the data which obey to Weibull distribution. Based on the above considerations, the appropriate Weibull distribution may be derived from the Extreme *ddf* apparent activation energy values. The two parameter Weibull *ddf* has the form:

$$f_W\left(E_a\right) = \frac{\beta}{\eta}\left(\frac{E_a}{\eta}\right)^{\beta-1} \exp\left[-\left(\frac{E_a}{\eta}\right)^{\beta}\right], \tag{19}$$

where E_a represents the random variable. In general, η represents the 0.632-quantile of the Weibull distribution regardless of the value of β, since $F_W(E_a)$ = 1 – exp(-1) ≈ 0.632 for all β > 0. Note that the spread of the Weibull distributions around η gets smaller as β increases.

The parameter η is also calls the *characteristic life* of the process, which obeys to the Weibull probability. The term "*life*" originates from the use of the probability functions in modeling the lifetime data. Taking into account obtained values of the Extreme distribution parameters (parameters μ and σ), the corresponding parameters (the shape and the scale

parameters) of the Weibull distribution were calculated, and they are as follows: β = 4.76 and η = 2.63525 × 10^{12} kJ mol^{-1}, respectively. Weibull *ddf* of apparent activation energy (E_a) values for static pyrolysis process is shown in Fig. 11, in the form of the energy bars.

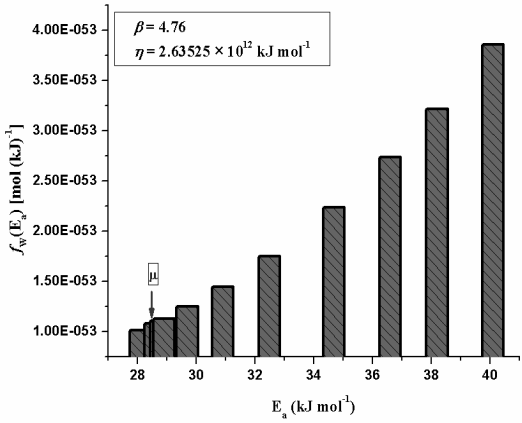

Figure 11. The Weibull *ddf* of the apparent activation energy values, for the static pyrolysis process of corn stover presented in the form of the energy bars. The Weibull distribution parameters are also given in the figure, with a marked position of the mean value (μ).

It can be seen from Fig. 11 that with $\beta >> 1$, the Weibull distribution has a pyrolysis rate that increases with time, but if η is increased, while β is kept the same, the distribution gets stretched out to the right (as in Fig. 9 (b)) for Extreme *ddf*), and its height decreases. In our case, we have high β value and very high value of η (×10^{12} kJ mol^{-1} (Fig. 11)), so that the Extreme distribution (Fig. 9 (b)) is transformed and changing its shape which is more exponential, whereby losing maximum (Fig. 11). Considering this transformation, which indicates that the expansion of the distribution goes to the infinity, which means that more and more new reactions then takes part in a complex scheme of pseudo-components decompositions, and this largely depends on the operating temperature.

It should be noted that the maximum density of E_a values is concentrated just around the mean value (indicated in Fig. 11) and which is near the maximum value in Fig. 9 (b). Namely, the gas yield in corn stover pyrolysis originates from decomposition processes of organic substances comprising many independent reactions, where each of them can be attributed to the corresponding value of E_a. In this sense, from a statistical point of view, we have that minimum of independent, "identically" distributed E_a values (as random variables)

(not necessarily Weibull distributed) has an *approximate* Weibull distribution, subject to some mild conditions concerning the distribution of such random variables. This assertion can be seen from the following standpoint: A sample of corn stover material can be viewed as a concatenation (a series of interconnected events) of "many smaller material cells" (these cells represent the biomass pseudo-components as cellulose, hemicelluloses and lignin) each of which has its random breaking energy E_i when subjected to thermal stress. Thus, the strength of the concatenated 'entire system' is the strength of its weakest link, namely $min(E_1, E_2, \ldots, E_N)$, i.e. approximately Weibull. On the other hand, the tested pyrolysis system can be viewed as a collection of subsystems (cellulose, hemicelluloses and lignin), each of which has the random lifetime.

Also, it should be pointed out that process which exhibits random pyrolysis times between micro-thermally induced shocks shows exponentially distributed reactivity with mean value tagged with μ.

In addition, for presented Weibull parameters (Fig. 11), we have that the part of the system subjected to thermal aging represents the less stable pseudo-component, whereby it has a higher chance of decomposition during small time increment, than the next stable pseudo-component. For tested sample, in pyrolysis process within considered operating temperature range, the hemicelluloses decompose firstly and then break down cellulose. Lignin is the last decomposes with a prolonged degradability process since this compound has high stability. The hemicelluloses, particularly its pentosans it can be argued that the first decomposed (its E_a amounts 20.8 kJ mol^{-1} [61], which is in excellent agreement with obtained mean value (28.6 kJ mol^{-1})) in operating temperature range of ΔT = 180 – 260 ^{o}C, followed by cellulose decomposition at 230/240 ^{o}C, and finally decomposition of lignin takes place at 270 ^{o}C. The scission of a carbon-to-oxygen bond in a pentose might lead to further splitting to acetic acid and perhaps formaldehyde or CO and H_2. Pentoses may yield furfural and other furan derivatives. This production can occur readily by dehydration to which carbohydrates are highly susceptible. Therefore, hemicelluloses evolve more gases, but giving less tar. During cellulose decomposition, some of carbon-to-oxygen bonds in links between glucosan units may be expected to break at random points along the chain, producing elevation in E_a values, and also resulting in an increase in the reactivity and therefore the likelihood of its occurring (as depicted in Fig. 11).

It is possible that initial break in carbon-to-oxygen chain links may occur by the random pyrolytic scission instead of hydrolysis.

At the observed operating temperatures of the pyrolysis, the transitory existence of free radicals that can then participate in the chain reactions is highly probable. Among such possible free radicals are the follows: CHO, CH_3, CH_2, H and OH. Because of their short lifetimes, they could not be found as the pyrolysis products, but they strongly affect on the course of the pyrolysis processing reactions.

If the free radicals may exist long enough in the vapors from pyrolyzed sample, they can participate in the autocatalytic increase in the reaction rate but can not continue infinitely. Then, it may be possible recombination and their concentration reaches the stationary state.

On the other hand, due to the higher ash content in corn stover sample (Table 1), the lower values of E_a may arise from the catalytic effect of the ash, changing the chemical structure of the biomass and the decomposition rate. The appearance of the autocatalytic properties of studied biomass system during pyrolysis was mechanistically described earlier.

4.5.1 Prediction model analysis

Based on the established model, we can use the Extreme (and then the approximate Weibull) distribution of E_a values to describe the distribution of reactivity for the actual pyrolysis process, in a form of the differential rate equation as:

$$\left(\frac{d\alpha}{dt}\right)_{CS} = \alpha^{M}\left(1-\alpha\right)^{N} \times \int_{0}^{\infty} \left[c_1 \underbrace{A_1 \exp\left(-\frac{E_{a1}}{RT}\right)}_{k_1(E_{a1})} + c_2 \underbrace{A_2 \exp\left(-\frac{E_{a2}}{RT}\right)}_{k_2(E_{a2})} \right] \times f\left(E_a\right) dE_a, \qquad (20)$$

where term $\alpha^{M}(1-\alpha)^{N}$ is derived truncated autocatalytic kinetic model, with the SB kinetic exponents (M and N) presented in Table 5, at all the observed operating temperatures. The term $\int f(E_a)dE_a$ was introduced because of the scaling conditions (normalized to the unity) of the density distribution function of E_a values.

The subscripts "1" and "2" refer to the main biomass pseudo-components which are actively involved in pyrolysis process, where "1" is attached to holocellulose (hemicelluloses + cellulose) and "2" is attached to lignin; The Arrhenius parameters A_1, E_{a1} and A_2, E_{a2} are attributed to "1" and "2" dates.

The symbol "CS" is referred to corn stover, while c_1 and c_2 are the contributions of holocellulose and lignin, respectively. The computation procedure in solving of the Eq. (20) was carried out with Matlab® program.

The same program was used in solving the appropriate integral form of the Eq. (20) for obtaining the overall conversion curves, with an approximate Weibull distribution. As a quality fitting parameter, the sum of square of relative error (SSRE) was implemented.

Table 6 shows the kinetic parameters from fitting procedure using overall rate equation presented through Eq. (22) and transformed differential equation into integral (conversion) curves, for tested pyrolysis process at various operating temperatures. The values of maximum error are also listed in Table 6.

Table 6. The parameters obtained by an advanced distributed reactivity model, implemented for the static pyrolysis process.

Distributed reactivity model for CS static pyrolysis in operating temperature range of ΔT = 180 °C – 270 °C				**Exreme *ddf* (Rate curves)**	**Weibull approximate *ddf* (Conversion, α–t — integral curves)**
				Maximum error	**Maximum error**
***T* (°C)**	**c_i in (%)**	**A_i (min^{-1})**	**E_{ai} (kJ mol^{-1})**	**(%)[b]**	**(%)[c]**
180	1 [52.8][a]	7.414×10^2	30.9 ± 0.3	3.29	3.15
	2 [47.2]	1.265×10^3	38.6 ± 0.5	3.03	3.21
230	1 [39.4]	4.896×10^2	32.3 ± 0.2	3.12	3.19
	2 [60.6]	2.996×10^3	39.4 ± 0.6	3.20	3.42
270	1 [49.7]	8.564×10^2	35.1 ± 0.3	3.03	2.89
	2 [50.3]	4.014×10^3	41.0 ± 0.7	3.22	3.34

[a] [...] is the percentage contribution.

[b] Average max. error value: 3.15 %.

[c] Average max. error value: 3.20 %.

The estimated kinetic (Arrhenius) parameters for mechanically selected kinetic model are in excellent agreement with previously established results. It can be observed that contributions of identified pseudo-components vary with the operating temperature and generally are not equal, which greatly depends on the composition of analyzed sample.

Fig. 12 (a)–(b) show comparison between experimental and observed rate pyrolysis curves from Extreme distribution of reactivity, and experimentally obtained conversion curves and the observed ones for the approximate Weibull distribution of reactivity, respectively.

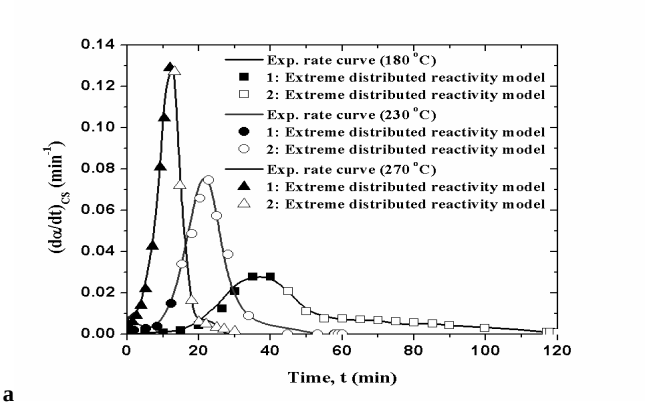

a

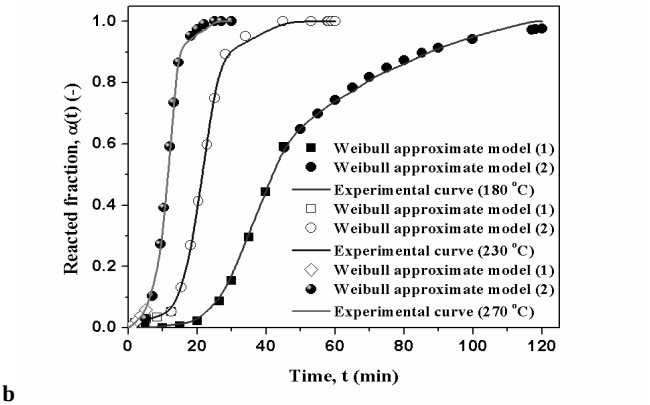

b

Figure 12. (a)–(b). Comparison between experimental and the observed rate pyrolysis curves from the Extreme distribution of reactivity, and experimentally obtained conversion ($\alpha - t$) curves and the observed ones for the approximate Weibull density distribution, respectively.

From Fig. 12 (a)-(b) we can see that there is very good agreement between experimental and calculated differential and integral kinetic curves using Extreme distributed reactivity model, together with Weibull distribution of reactivity, which represents excellent approximation for describing the static pyrolysis of corn stover. This model is high appreciated for corn stover biomass material, because it shows excellent performance, bearing in mind that the maximum deviation is around 3.00 % (Table 6).

Newly proposed distributed reactivity model can identify the key species which can be used as marker compounds to recognize spontaneous reaction regimes in low-temperature

pyrolysis of lignocellulosic material, enabling design of more energy efficient industrial thermo-chemical processes.

5 Concluding remarks

This work provides a new distributed reactivity model for investigation of static pyrolysis of agricultural residues based on lignocellulosic constituents. As an testing system, the corn stover biomass sample was chosen for pyrolysis measurements. It was found that at lowest operating temperature (180 ^{o}C), the pyrolysis process was governed by autocatalytic and non-autocatalytic reactions which occur simultaneously. With an increasing of operating temperature above 180 ^{o}C, the amplifying of acceleratory behavior of the process was observed, where at 270 ^{o}C a fairly rapid surface reactions dominate. It was established that surface reaction geometry activities become dominant at highest operating temperature. Due to existence of transient nucleation that implies negative deviation from universal kinetic parameter value, especially at high operating temperatures, it has been found that Avrami-Erofeev model fails in physical description of current process. It was found that distributed reactivity model which includes Šestak-Berggren kinetic model with combined Extreme and Weibull (as approximate) distributions of apparent activation energy values can fully describe the pyrolysis process. Proposed reactivity model can identify most important species which can be used as marker compounds to recognize spontaneous reaction regimes during the process.

Acknowledgement: This research work was partially supported by the Serbian Ministry of Education, Science and Technological Development under the project numbered III42010, 172015 and TR37021.

References

[1] G. W. Huber, S. Iborra, A. Corma, Synthesis of transportation fuels from biomass: Chemistry, catalysis, and engineering, *Chem. Rev.* **106** (2006) 4044–4098**.**

[2] L. Wang, C. L. Weller, D. D. Jones, M. A. Hanna, Contemporary issues in thermal gasification of biomass and its application to electricity and fuel production, *Biomass Bioenergy* **32** (2008) 573–581.

[3] P. Chartier, G.L. Ferrero, V.M. Henius, S. Hultberg, J. Sachau, M. Wiinblad, *Biomass for Energy and the Environment*, Pergamon, New York, 1997, pp. 501–507.

[4] D. C. Dayton, H. L. Chum, Symposium on biomass fuels: The introduction, *Energy Fuels* **10** (1996) 267–268.

[5] D. Wang, S. Czernik, D. Montané, M. Mann, E. Chornet, Biomass to hydrogen *via* fast pyrolysis and catalytic steam reforming of the pyrolysis oil or its fractions, *Ind. Eng. Chem. Res*. **36** (1997) 1507–1518.

[6] A. Aqsha, N. Mahinpey, T. Mani, F. Salek, P. Murugan, Study of sawdust pyrolysis and its devolatilisation kinetics, *Can. J. Chem. Eng*. **89** (2011) 1451–1457.

[7] F. Ma, Y. Zeng, J. Wang, Y. Yang, X. Yang, X. Zhang, Thermogravimteric study and kinetic analysis of fungal pretreated corn stover using the distributed activation energy model, *Bioresour. Technol*. **128** (2013) 417–422.

[8] M. Asadieraghi, W. M. Ashri Wan Daud, Characterization of lignocellulosic biomass thermal degradation and physiochemical structure: Effects of demineralization by diverse acid solutions, *Energy Conv. Manag*. **82** (2014) 71–82.

[9] Y. Ding, O. A. Ezekoye, S. Lu, C. Wang, Thermal degradation of beech wood with thermogravimetry/Fourier transform infrared analysis, *Energy Conv. Manag*. **120** (2016) 370–377.

[10] S. A. Arni, Comparison of slow and fast pyrolysis for converting biomass into fuel, *Renew*. *Energy* **124** (2018) 197–201.

[11] P. Bartocci, R. Tschentscher, R. E. Stensrød, M. Barbanera, F. Fantozzi, Kinetic analysis of digestate slow pyrolysis with the application of the master-plots method and independent parallel reactions scheme, *Molecules* **24** (2019) #1657.

[12] P. Yangali, A.M. Celaya, J. L. Goldfarb, Co-pyrolysis reaction rates and activation energies of West Virginia coal and cherry pit blends, *J. Anal. Appl. Pyrol*. **108** (2014) 203–211.

[13] C. Branca, C. Di Blasi, Kinetics of the static degradation of wood in the temperature range 528-708 K, *J. Anal. Appl. Pyrol*. **67** (2003) 207–219.

[14] K. Hashimoto, I. Hasegawa, J. Hayashi, K. Mae, Correlations of kinetic parameters in biomass pyrolysis with solid residue yield and lignin content, *Fuel* **90** (2011) 104–112.

[15] A. K. Burnham, R. L. Braun, Global kinetic analysis of complex materials, *Energy Fuels* **13** (1999) 1–22.

[16] K. Q. Tran, H. H. Bui, W. H. Chen, Distributed activation energy modelling for thermal decomposition of microalgae residues, *Chem*. *Eng*. *Trans*. **50** (2016) 175–180.

[17] A. Dhaundiyal, S. B. Singh, Distributed activation energy modelling for pyrolysis of forest waste using Gaussian distribution, *Proc. Latv. Acad. Sci. B* **70** (2016) 64–70.

[18] J. Cai, R. Liu, New distributed activation energy model: Numerical solution and application to pyrolysis kinetics of some types of biomass, *Bioresour*. *Technol*. **99** (2008) 2795–2799.

[19] S. Vyazovkin, K. Chrissafis, M. L. Di Lorenzo, N. Koga, M. Pijolat, B. Roduit, N. Sbirrazzuoli, J. J. Sunol, ICTAC kinetics committee recommendations for collecting experimental thermal analysis data for kinetic computations, *Thermochim. Acta* **590** (2014) 1–23.

[20] A. Sharuddin, F. Abnisa, D. Wan, M. Aroua, A review on pyrolysis of plastic wastes, *Energy Conv. Manag.* **115** (2016) 308–326.

[21] N. Kaliyan, R. V. Morey, Densification characteristics of corn stover and switchgrass, *Trans. ASABE* **52** (2009) 907–920.

[22] *ASTM International D3173*. Standard Test Methods for Moisture in the Analysis Sample of Coal and Coke, 2008, The last modified 2015. http://www.astm.org/Standards/D3173.htm

[23] *ASTM International D3174*. Standard Test Methods for Ash Analysis of Coal and Coke, 2002, The last modified 2015. http://edis.ifas.ufl.edu/pdffiles/AG/AG29600.pdf

[24] *ASTM International D3175*. Standard Test Methods for Volatile Matter in the Analysis Sample od Coal and Coke, 2007, The last modified 2015. http://www.astm.org/Standards/D3175.htm

[25] *ASTM International D3177*. Standard Test Methods for Total Sulfur in the Analysis Sample of Coal and Coke, 2002. The last modified 2015. http://www.astm.org/Standards/D3177.htm

[26] *ASTM International D3178*. Standard Test Methods for Carbon and Hydrogen in the Analysis Sample of Coal and Coke, 2002, The last modified 2015. http://www.astm.org/Standards/D3178.htm

[27] *ASTM International D3179*. Standard Test Methods for Nitrogen in the Analysis Sample of Coal and Coke, 2002, The last modified 2015. http://www.astm.org/Standards/D3179.htm

[28] *ASTM International D5865*. Standard Test Methods for Gross Calorific Value of Coal and Coke, 2010, The last modified 2015. http://www.astm.org/Standards/D5865.htm

[29] S. Vyazovkin, Model-free kinetics, *J. Therm. Anal. Calorim*. **83** (2006) 45–51.

[30] B. Ramajo-Escalera, A. Espina, J. R. García, J. H. Sosa-Arnao, S. A. Nebra, Model-free kinetics applied to sugarcane bagasse combustion, *Thermochim. Acta* **448** (2006) 111–116.

[31] F. Baitalow, H. G. Schmidt, G. Wolf, Formal kinetic analysis of processes in the solid state, *Thermochim. Acta* **337** (1999) 111–120.

[32] H. L. Friedman, Kinetics of thermal degradation of char-forming plastics from thermogravimetry – Application to a phenolic resin, *J. Polym. Sci. C* **6** (1964) 183–195.

[33] J. Málek, Kinetic analysis of crystallization processes in amorphous materials, *Thermochim. Acta* **355** (2000) 239–253.

[34] M. Avrami, Kinetics of phase change. I. General theory, *J. Chem. Phys*. **7** (1939) 1103–1112.

[35] J. D. Hancock, J. H. Sharp, Method of comparing solid-state kinetic data and its application to the decomposition of kaolinite, brucite and $BaCO_3$, *J. Am. Ceram. Soc*. **55** (1972) 74–77.

[36] M. A. Gibson, G. W. Delamore, Crystallization kinetics of some iron-based metallic glasses, *J. Mater. Sci*. **22** (1987) 4550–4557.

[37] J. Vázquez, D. García-G. Barreda, P. L. López-Alemany, P. Villares, R. Jiménez-Garay, A study on non-static transformation kinetics: Application to the crystallization of the $Ge_{0.18}Sb_{0.23}Se_{0.59}$ glassy alloy, *Mater. Chem. Phys*. **96** (2006) 107–115.

[38] M. Tomellini, M. Fanfoni, Impingement factor in the case of phase transformations governed by spatially correlated nucleation, *Phys. Rev. B* **78** (2008) 014206–014215.

[39] J. Cai, W. Wu, R. Liu, G.W. Huber, A distributed activation energy model for the pyrolysis of lignocellulosic biomass, *Green Chem*. **15** (2013) 1331–1340.

[40] G. Várhegyi, B. Bobály, E. Jakab, H. Chen, Thermogravimetric study of biomass pyrolysis kinetics. A distributed activation energy model with prediction tests, *Energy Fuels* **25** (2011) 24–32.

[41] B. de Caprariis, M.L. Santarelli, M. Scarsella, C. Herce, N. Verdone, P. De Filippis, Kinetic analysis of biomass pyrolysis using a double distributed activation energy model, *J. Therm. Anal. Calorim*. **121** (2015) 1403–1410.

[42] K. Miura, T. Maki, A simple method for estimating $f(E)$ and $k_0(E)$ in the distributed activation energy model, *Energy Fuels* **12** (1998) 864–869.

[43] A. Zabaniotou, O. Ioannidou, Evaluation of utilization of corn stalks for energy and carbon material production by using rapid pyrolysis at high temperature, *Fuel* **87** (2008) 834–843.

[44] J. Fernandez-Cornejo, S. Wechsler, M. Livingston, L. Mitchell, *Genetically Engineered Crops in the United States. United States Department of Agriculture*, Economic Research Service, Economic Research Report, Washington, 2014, p. 1–60.

[45] Y. F. Huang, W.-H. Kuan, C. C. Chang, Y. M. Tzou, Catalytic and atmospheric effects on microwave pyrolysis of corn stover, *Bioresour. Techn*. **131** (2013) 274–280.

[46] A. Demirbas, Calculation of higher heating values of biomass fuels, *Fuel* **76** (1997) 431–434.

[47] W. W. Wilhelm, J. M. F. Johnson, D. T. Lightle, D. L. Karlen, J. M. Novak, N. W. Barbour, D. A. Laird, J. Baker, T. E. Ochsner, A. D. Halvorson, F. Arriaga, N. Barbour, Vertical distribution of corn stover dry mass grown at several US locations, *Bioenergy Res*. **4** (2011) 11–21.

[48] W. C. Edens, L. O. Pordesimo, S. Sokhansanj, Field drying characteristics and mass relationships of corn stover fractions, *ASAE* (2002) #026015.

[49] DOE, United States Department of Energy. Biomass feedstock composition and property database. Department of Energy, Biomass Program, 2006, Available at the website: http://www.eere.energy.gov/biomass/progs/search1.cgi

[50] G. K. Mansaray, A. E. Ghaly, Determination of kinetic parameters of rice husks in oxygen using thermogravimetric analysis, *Biomass Bioenergy* **17** (1999) 19–31.

[51] M. G. Grønli, M. C. Melaaen, Mathematical model for wood pyrolysis comparison of experimental measurements with model predictions, *Energy Fuels* **14** (2000) 791–800.

[52] A. V. Bridgwater, Renewable fuels and chemicals by thermal processing of biomass, *Chem. Eng. J*. **91** (2003) 87–102.

[53] H. B. Vuthaluru, Investigations into the pyrolytic behaviour of coal/biomass blends using thermogravimetric analysis, *Bioresour. Techn*. **92** (2004) 187–195.

[54] G. Lv, S. Wu, Analytical pyrolysis studies of corn stalk and its three main components by TG-MS and Py-GC/MS, *J. Anal. Appl. Pyrol*. **97** (2012) 11–18.

[55] Y. Du, X. Jiang, G. Lv, X. Li, Y. Chi, J. Yan, X. Liu, A. Buekens, TG-pyrolysis and FTIR analysis of chocolate and biomass waste, *J. Therm. Anal. Calorim*. **117** (2014) 343–353.

[56] M. Poletto, V. Pistor, R. M. Campomanes Santana, A. José Zattera, Materials produced from plant biomass. Part II: Evaluation of crystallinity and degradation kinetics of cellulose, *Mater. Res*. **15** (2012) 421–427.

[57] J. Šesták, G. Berggren, Study of the kinetics of the mechanism of solid-state reactions at increased temperature, *Thermochim. Acta* **3** (1971) 1–12.

[58] S. Vyazovkin, A. K. Burnham, J. M. Criado, L. A. Pérez-Maqueda, C. Popescu, N. Sbirrazzuoli, ICTAC Kinetics Committee recommendations for performing kinetic computations on thermal analysis data, *Thermochim. Acta* **520** (2011) 1–19.

[59] S. Kotz, S. Nadarajah, *Extreme Value Distributions*. *Theory and Applications*, Imperial College Press, London, 2000, pp. 61–95.

[60] A. Demirbas, Combustion characteristics of different biomass fuels, *Prog. Energy Comb*. *Mater*. **30** (2004) 219–230.

[61] C. L. Wright, *Effect of Harvest Method on the Nutrient Composition of Baled Cornstalks*, South Dakota State Univ., Brookings, 2005, pp. 46–47.